CICERO Simple Climate Model (CICERO-SCM v1.1.1) – an improved simple climate model with a parameter calibration tool

Marit Sandstad[1], Borgar Aamaas[1], Ane Nordlie Johansen[1], Marianne Tronstad Lund[1], Glen P. Peters[1], Bjørn Hallvard Samset[1], Benjamin Mark Sanderson[1], Ragnhild Bieltvedt Skeie[1]

5   [1] CICERO Center for International Climate Research, Oslo 0349, Norway

Correspondence to: Marit Sandstad (marit.sandstad@cicero.oslo.no)

Abstract. The CICERO Simple Climate Model (CICERO-SCM) is a lightweight, semi-empirical model of global climate. Here we present a new open-source Python port of the model for use in climate assessment and research. The new version of CICERO-SCM has the same scientific logic and functionality as the original FORTRAN version but it is considerably more
10   flexible and open source via Github. We describe the basic structure, improvements compared to the previous FORTRAN version, together with technical descriptions of the global thermal dynamics and carbon cycle components and the emissions module, before presenting a range of standard figures demonstrating its application. A new parameter calibration tool is demonstrated to make an example calibrated parameter set to span and fit a simple target specification. CICERO-SCM is fully open source and available through GitHub (https://github.com/ciceroOslo/ciceroscm).

15   ## 1 Introduction

Simple Climate Models (SCMs), also termed Reduced-Complexity Models (RCMs), have an important role in climate modelling. While Earth System Models (ESMs) are used to resolve climate processes on a resolved grid, they remain extremely resource intensive, however, much simpler models can reproduce key globally aggregated outputs (e.g., globally averaged surface temperature) (Balaji et al., 2017; Schneider and Thompson, 1981; Wigley and Raper, 1992). Thus, simple
20   models can be used to both help understand and explain physical processes (e.g. Peters et al., 2011) or be calibrated to replicate the behaviour and uncertainty across a range of more complex ESMs (Meinshausen et al., 2011). SCMs can be used to estimate the climate uncertainties across thousands of emissions scenarios in a short run time (Kikstra et al., 2022), something which remains impossible for ESMs with today's computing power, and have been used to quantify uncertainty in key climate indicators such as climate sensitivity (Sherwood et al., 2020) and the remaining carbon budget (Lamboll et al.,
25   2023).

Even though SCMs can be used to emulate more complex models, there remains value in maintaining a diversity of SCMs because the reduced form representation of the climate often rests on a set of structural assumptions and modeling philosophies which limit the response of the model (Nicholls et al., 2021, 2020). SCMs can exhibit a wide range of complexity, ranging from simple one- or two-layer energy-balance models which are used in the operational calculation of

30 emission metrics (Aamaas et al., 2013) up to more comprehensive representation of the carbon cycle and energy balance (e.g. (Gasser et al., 2020; Meinshausen et al., 2011)). There are also Intermediate Complexity Models, sitting somewhere between an SCM and ESM, but for the purpose of this article, we consider SCMs to be models which allow simulation of a scenario on a single CPU in seconds or less.

The different complexity levels of SCMs can lead to different outcomes when key physical processes are constrained from
35 data, such as tradeoffs in climate forcers, and carbon-climate feedbacks on different time scales, such that models with different structures constrained on the same data can exhibit different future constrained projection distributions (Jenkins et al., 2021; Kikstra et al., 2022; Lamboll et al., 2023). While SCMs can be calibrated to replicate the behaviour of more complex models, there is also a diversity of ways to do this. Calibration could be done only on the historical period using observational based data (e.g., (Aldrin et al., 2012)), or on complex model simulations over longer time periods using
40 scenarios (e.g., out to 2100, (Meinshausen et al., 2011)) or using idealized simulations (e.g. response to abrupt or gradual changes in CO_2 concentration) (Olivié and Stuber, 2010). Further, different variables could be used in the calibration, such as concentrations, surface temperature, and ocean heat content (Smith et al., 2021b). Subjective calibration choices can also lead to differences in climate outcomes (Sanderson, 2020). Each level of model complexity and calibration method has advantages and disadvantages, and to ensure robust and policy relevant results, it is necessary to maintain and develop a
45 range of SCMs.

The original version of the CICERO[1] Simple Climate Model (CICERO-SCM) was developed in 1999 (Fuglestvedt and Berntsen, 1999) to study the effects of future emissions on global mean surface temperature and sea level rise. Atmospheric carbon dioxide (CO_2) was estimated using an ocean mixed-layer pulse response function (Alfsen and Berntsen, 1999; Joos
50 and Bruno, 1996). The response to other long lived greenhouse gas emissions were estimated using simple first-order decay equations, and the radiative forcing was estimated using simple proportionality between concentration and forcing for each gas. Direct and indirect radiative forcing of aerosols, radiative forcing of tropospheric and stratospheric ozone (O_3) and stratospheric water vapor were implemented using simplified expressions. The total radiative forcing provided boundary conditions for an energy-balance upwelling-diffusion ocean model (Schlesinger et al., 1992). A time-varying lifetime of
55 methane (CH_4) was introduced after the IPCC (Integovernmental Panel on Climate Change) Third Assessment Report based on a linear interpolation of the changes in the hydroxyl radical (OH) concentration with CH_4 concentration, nitrogen oxides (NOx), carbon monoxide (CO) and non-methane volatile organic carbon (NMVOC) emissions (table 4.11 footnote b of (Ehhalt et al., 2001)). Since then, the core structure of the CICERO-SCM has remained relatively unchanged, though parameters have been constantly updated in line with the best available science. The model has been used in a range of

---

1 [1] **CICERO Center for International Climate Research**

60 studies, such as, historical contributions to global warming (den Elzen et al., 2005, 2013; Höhne et al., 2011; Skeie et al., 2017, 2021), global warming from different economic sectors (Skeie et al., 2009; Tronstad Lund et al., 2012) estimates of the climate sensitivity (Aldrin et al., 2012; Skeie et al., 2014, 2018), simple model intercomparisons (Nicholls et al., 2021, 2020) and assessment of specific mitigation strategies (Myhre et al., 2011; Torvanger et al., 2012, 2013). The CICERO-SCM was also used in the IPCC Sixth Assessment Report (Guivarch et al., 2022; Kikstra et al., 2022; Smith et al., 2021b).

65 In this article we describe and assess an updated version of the CICERO-SCM, now written in Python and made openly accessible to encourage community development and engagement. The model has also been supplemented with features for parameter calibration, and easier parallel runs.

2 Model structure

70
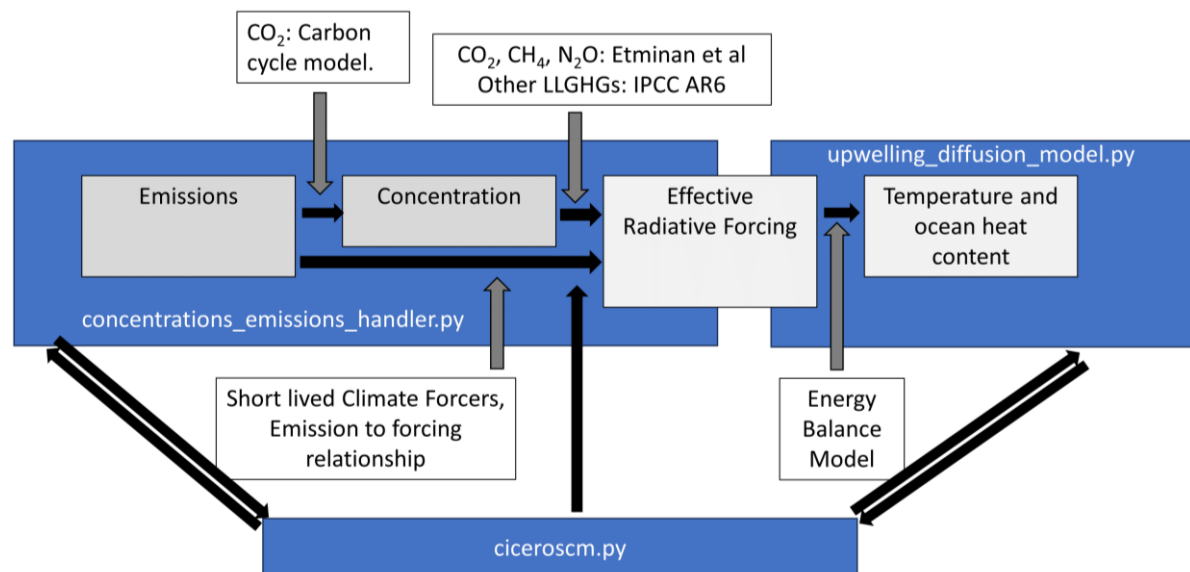
Figure 1: The core model structure. The *concentrations_emissions_handler.py* module calculates concentrations from emissions using a carbon cycle model for atmospheric CO₂ and first order decay equations for other components. It then calculates forcing from concentrations using the (Etminan et al. 2016) scheme for CO₂, CH₄ and N₂O, and updated proportionality relationships for other gases. Simplified expressions calculate forcing directly from emissions for aerosols, O₃ and stratospheric water vapour. The
75 **effective radiative forcing is passed to the *upwelling_diffusion_model.py* where it is used as input to the ocean energy balance model (Schlesinger, Jiang, and Charlson 1992) to calculate temperature and ocean heat content. This process is repeated for each time step, and looping and information passing is handled by the ciceroscm.py control module.**

Figure 1 shows the overall structure and flow of the CICERO-SCM. The core of the model consists of one module, *concentrations_emissions_handler.py* (see section 2.1), which calculates concentrations from emissions, and forcing from
80 concentrations or directly from emissions, and another module, *upwelling_diffusion_model.py*, which calculates temperature from forcing, using an upwelling diffusion energy balance model (UDM/EBM) (see section 2.2). A main control module,

ciceroscm.py, calls these two, transfers data from the emissions to forcing module to upwelling diffusion module, loops over years, and takes care of outputs. The model can be run directly from input concentrations or forcing time series, in addition to running all the way from emissions to temperatures. Inputs and outputs are all global and on yearly time resolution with

85 some exceptions. The *upwelling_diffusion_model.py* has two hemispheres and does calculations using 12 sub yearly timesteps to ensure convergence. The forcing input is therefore for two hemispheres. Volcanic forcing input is on a monthly time resolution (see section 2.2 and Appendix C for further details). The carbon cycle uses 24 sub yearly timesteps to integrate the carbon response, however, inputs and outputs only yearly values (see section 2.1.1). In section 2.3 we describe the main differences between the new Python port version and the previous FORTRAN implementation.

90

The code also includes various modules and help functions to handle perturbations (*perturbations.py*), utilities used by multiple modules (*pub_utils.py* and *_utils.py*), handling of input in various formats (*input_handler.py*) and making default summary plots (*make_plots.py*). It also ships with a subpackage for handling parallel runs including a parallelization wrapper (*cscmparwrapper.py*), a module to define a distribution run (*distributionrun.py*) and modules to build and define a

95 distribution and do calibration (*_configdistro.py* and *calibrator.py*). All these tools will be described in more detail in section 2.4.

A regular run of the code will start by defining a CICERO-SCM instance, that can then be used to run the model for the same experiment, but with various parameter values. Table 1 shows the parameters for creation of such an instance. A

100 default run will lead to output files being generated, but the outputs can also be held in a dictionary with separate keys and corresponding values for outputs from the *upwelling_diffusion_model.py* and additional keys for datasets for concentration, emissions and forcing. A run can also produce automatic plots. Appendix A contains figures showing the automatic plots generated from a default configuration emission to forcing run of the CMIP6 historical experiment (Figs. A1-A11).

Name	Description
Mandatory parameters	
gaspam_file	List of gases and aerosols to be used in the model. See also Table 3.
Optional parameters	
Sunvolc	Parameter to include solar and volcanic forcing. If set to 1, they will be included, see section 2.1.12. Datasets for this forcing can be supplied by the user or taken from defaults that come with the model.
rf_sun_file	Path to solar forcing file, see section 2.1.12
rf_volc_file	Path to volcanic forcing file, see section 2.1.12

perturb_forc_file	Forcing timeseries to be added as a perturbation to the forcing timeseries calculated from the concentrations_emissions_handler. See section 2.1.13 for details.
perturb_em_file	Emissions timeseries to be added as a perturbation to emissions from a predefined emissions file. See section 2.1.13 for details.
Parameters for concentrations or emissions configurations	
concentrations_file	File with concentration timeseries of gases. Used in concentration driven run. For emission driven run, the pre-industrial values from this file is used and the values from nystart to emstart for all gases except CO_2.
emissions_file	File with emission timeseries of gases. (Used even in concentration driven runs for short lived climate forcers)
nat_ch4_file	File with natural emissions of CH_4. See section 2.1.3 for details
nat_n2o_file	File with natural emissions of N_2O. See section 2.1.4 for details
Idtm	Sub yearly timesteps in concentration emission model, used to calculate the CO_2 concentrations from emissions.
Nystart	Start year of the run
Nyend	End year of the run
Emstart	Emissions start year, with concentrations used between nystart and emstart if they are different
rs_function	Custom mixed layer pulse response function. Argument must be a function that takes in step number and idtm, can be generated from an array using make_rs_function_from_arrays in pub_utils. See section 2.1.1 for description of default value and use.
rb_function	Custom mixed layer pulse response function. Argument

	must be a function that takes in step number and idtm, can be generated from an array using make_rb_function_from_arrays in pub_utils. See section 2.1.1 for description of default value and use
conc_run	Optional Boolean parameter too specify that the run is meant as a concentration driven run.
Parameters for a pure forcing configuration	
forc_file	Can be single column of data, contain years as a column, have forcings per various forcing components, or contain columns for FORC_NH and FORC_SH for a hemispherically split of forcing

Table 1: Parameters used in defining a ciceroscm model object.

2.1 Emissions to radiative forcing – concentrations_emissions_handler

The module *concentrations_emissions_handler.py* calculates the effective radiative forcing time series. Each timestep this is done by first calculating concentrations from emissions. In a concentration driven run, this is done by simply reading the concentrations in. Otherwise, a carbon cycle described in section 2.1.1 is employed to calculate the CO_2 concentrations, a mass balance equation is used for the other components as described in section 2.1.2, with special modifications to account for multiple decay processes and natural emission for CH_4 (section 2.1.3) and nitrous oxide (N_2O) (section 2.1.4). When concentrations have been calculated, forcing is derived. For this, the scheme described in (Etminan et al., 2016) is first used to calculate the forcing from CO_2, CH_4 and N_2O (section 2.1.5). Then looping over all other chemical components, forcing will be calculated using tabulated concentrations to forcing values (section 2.1.6) or calculated specifically for various species (see section 2.1.7 for tropospheric O_3, section 2.1.8 for stratospheric O_3, 2.1.9 for stratospheric water vapour, for aerosol forcing, 2.1.10 for albedo from land use change, 2.1.11 for aerosol forcing and 2.1.12 for solar and volcanic forcing).

Inputs to the module (Table 1) are files or datasets of emission and concentrations time series (Table 1), a file or dataset to define what gases and substances to consider, and optional integers to define the start year, end year, year at which to start running from emissions, number of sub yearly timesteps for carbon cycle calculations and a Boolean option to make the runs pure concentrations runs. Additional optional parameters giving files or datasets for natural emissions of CH_4 and N_2O and custom pulse response functions for the carbon cycle model can also be passed.

Some concentrations data are needed even in emissions-driven mode for pre-industrial concentrations and to define concentrations prior to the chosen year of emission start. The default year of run start is 1750, the model uses CO_2 emissions

from the outset, whereas non-CO_2 emissions start in the emissions start year, default year in 1850, so up to the year of emission start all other components have forcing calculated directly from concentrations. After the emissions start, all components will have forcing calculated from emissions. Alternatively, the model can be configured to use prescribed concentrations for all gases for the duration of the run.

130 When the model is to be run, an array of parameters to control the properties of calculations can be adjusted. Table 2 shows these parameters, most of which control the forcing strength of various substances.

Parameter	Default value	Unit	Description
qbmb	0.0	W m^{-2}	Biomass burning aerosol forcing in ref_yr. Scaled using the amount of biomass burning organic carbon (BMB_AEROS_OC)
qo3	0.5	W m^{-2}	Tropospheric O_3 forcing in ref_yr, see section 2.1.7
qdirso2	-0.36	W m^{-2}	Direct forcing sulphate in ref_yr, see section 2.1.10
qindso2	-0.97	W m^{-2}	Indirect RF sulphate in ref_yr, see section 2.1.10
qbc	0.16	W m^{-2}	BC (fossil fuel+biofuel) forcing in ref_yr, see section 2.1.10
qoc	-0.08	W m^{-2}	OC (fossil fuel+biofuel) forcing in ref_yr, see section 2.1.10
qh2o_ch4	0.091915		Forcing from CH_4 induced changes to stratospheric water vapour, see section 2.1.9
ref_yr	2010		Reference year for the forcing values above. To construct radiative forcing time series, these forcing values are scaled backwards and forwards using emissions. The forcing in ref_yr is equal to the forcing value above.
beta_f	0.287		Fertilisation factor in (Joos and Bruno, 1996) scheme carbon cycle, see section 2.1.1

			Option parameter that allows you to run the upwelling diffusion model with forcing from just a single component
just_one			Option parameter that allows you to run the upwelling diffusion model with forcing from just a single component
lifetime_mode			Lifetime mode for CH$_4$, valid options are "TAR" (table 4.11 footnote b of (Ehhalt et al., 2001), "CONSTANT_12" (for a constant value of 12 years) or "WIGLEY", a wigley exponent behaviour (Osborn and Wigley, 1994). "TAR" is the default but using a flat OH lifetime from the *gaspam*_file is a hidden default if you send a value for this option which is not "TAR" nor "CONSTANT_12" nor "WIGLEY". For details see section 2.1.3.

Table 2: Parameters to the *concentration_emissions_handler*

The *gaspam_file* or corresponding dataset defines which substances for the model to consider and includes properties defining the calculations to be performed for them. Table 3 shows the default shipped *gaspam_file* and its structure. Information from this file is used in the calculations of both concentrations from emissions and when mapping concentrations to forcing.

GAS	EM_UNIT	CONC_UNIT	BETA	ALPHA	TAU1(YEARS)	TAU2	TAU3	NATURAL_EMISSIONS	SARF_TO_ERF
CO2	Pg_C	ppm	2.123	0	150	0	0	0	1.05
CH4	Tg	ppb	2.78	0	9.6	120	160	275	0.877193
N2O	Tg_N	ppb	4.81	0	121	0	0	9.5	1.07
SO2	Tg_S	-	0	0	0	0	0	0	1
CFC-11	Gg	ppt	22.6	0.000259	52	0	0	0	1.13
CFC-12	Gg	ppt	20.8	0.00032	102	0	0	0	1.12
CFC-113	Gg	ppt	32.5	0.000301	93	0	0	0	1
CFC-114	Gg	ppt	29.7	0.000314	189	0	0	0	1

CFC-115	Gg	ppt	27.1	0.000246	540	0	0	0	1
CH3Br	Gg	ppt	16.4	0.000004	0.8	0	0	0	1
CCl4	Gg	ppt	25.3	0.000166	32	0	0	0	1
CH3CCl3	Gg	ppt	22	0.000065	5	0	0	0	1
HCFC-22	Gg	ppt	14.9	0.000214	11.9	0	0	0	1
HCFC-141b	Gg	ppt	26.3	0.000161	9.4	0	0	0	1
HCFC-123	Gg	ppt	20.1	0.00016	1.3	0	0	0	1
HCFC-142b	Gg	ppt	16.8852	0.000193	18	0	0	0	1
H-1211	Gg	ppt	28.37	0.0003	16	0	0	0	1
H-1301	Gg	ppt	25.55	0.000299	72	0	0	0	1
H-2402	Gg	ppt	45.9564	0.000312	28	0	0	0	1
HFC125	Gg	ppt	21.27	0.000234	30	0	0	0	1
HFC134a	Gg	ppt	18.09	0.000167	14	0	0	0	1
HFC143a	Gg	ppt	14.9	0.000168	51	0	0	0	1
HFC227ea	Gg	ppt	30.14	0.000273	36	0	0	0	1
HFC23	Gg	ppt	12.41	0.000191	228	0	0	0	1
HFC245fa	Gg	ppt	23.76	0.000245	7.9	0	0	0	1
HFC32	Gg	ppt	9.22	0.000111	5.4	0	0	0	1
HFC4310mee	Gg	ppt	44.68	0.000357	17	0	0	0	1
C2F6	Gg	ppt	24.46	0.000261	10000	0	0	0	1
C6F14	Gg	ppt	59.92	0.000449	3100	0	0	0	1
CF4	Gg	ppt	15.6	0.000099	50000	0	0	0	1
SF6	Gg	ppt	25.89	0.000567	3200	0	0	0	1
NOx	Mt_N	-	0	0	0	0	0	0	1
CO	Mt	-	0	0	0	0	0	0	1
NMVOC	Mt	-	0	0	0	0	0	0	1
NH3	Mt	-	0	0	0	0	0	0	1
SO4_IND	X	-	0	0	0	0	0	0	1
TROP_O3	X	-	0	0	0	0	0	0	1
STRAT_O3	X	-	0	0	0	0	0	0	1
STRAT_H2O	X	-	0	0	0	0	0	0	1

GAS	EM_UNIT	CONC_UNIT	BETA	ALPHA	TAU1	TAU2	TAU3	NATURAL_EMISSIONS	SARF_TO_ERF
BMB_AER OS_BC	Tg	-	0	0	0	0	0	0	1
BMB_AER OS_OC	Tg	-	0	0	0	0	0	0	1
BMB_AER OS	X	-	0	0	0	0	0	0	1
LANDUSE	X	-	0	0	0	0	0	0	1
BC	Tg	-	0	0	0	0	0	0	1
OC	Tg	-	0	0	0	0	0	0	1
OTHER	X	-	0	0	0	0	0	0	1

Table 3: The structure of the *gaspam_file*. In it, properties of greenhouse gases and short-lived climate gases or precursors used in calculations are defined. This is the standard shipped version of the gaspam_file, but the user is free to define their own file adding or subtracting gases and adjusting values for lifetimes, forcing strength and so on as they see fit. The column headers are: the name of the gas or substance in the run (GAS), emissions unit (EM_UNIT), concentration unit (CONC_UNIT), the conversion unit between concentration and mass (unit is the ratio of the emissions unit to the concentration unit) (BETA), radiative efficiency (ALPHA) in $W\ m^{-2}\ ppb^{-1}$, lifetime in years, in the case of CH_4 the lifetime is split into the OH lifetime in years (TAU1), soil lifetime in years (TAU2) and stratospheric lifetime in years (TAU3), natural emissions ((NATURAL_EMISSIONS) where the unit should be the same as the emissions unit , and a unitless conversion factor from stratospheric adjusted radiative forcing (SARF) to effective radiative forcing (ERF) (SARF_TO_ERF). In the current implementation, TAU2 and TAU3 are only used for CH_4 and the ALPHA parameter is unused for CO_2, CH_4, N_2O and aerosols. Gases with "–" in the CONC_UNIT column are not converted from emissions to concentrations and concentrations of these are not outputted or used in calculations. Gases with X in the emissions column are not read from the emissions files, but the forcing is calculated through other means from emissions of other components.

2.1.1 CO_2 – emissions to concentrations

The carbon cycle in the CICERO-SCM includes one part for the decay -of CO_2 into the deep ocean, and one part, for impacts from the terrestrial ecosystem.

The deep ocean sink is modelled using a scheme for CO_2 from (Joos et al., 1996) and an explanation of the CICERO-SCM implementation can be found in (Alfsen and Berntsen, 1999). The CO_2 module uses an a diffusive air-sea exchange model, combined with a decay function which represents transfer of carbon to the deep ocean (Alfsen and Berntsen, 1999; Siegenthaler and Joos, 1992). Atmospheric CO_2 partial pressures $\delta pCO_{2,a}(t)$, in ppm are calculated as follows:

$$\frac{d}{dt}\delta pCO_{2,a}(t) = \frac{e(t)-f_{fer}}{C_{\text{ppm\_to\_PgC}}} - A_{oc}f_{a,s} \tag{1}$$

Where e(t) are the total emissions at time t (in PgC yr^{-1}), f_{fer} is the net carbon uptake of the terrestrial carbon cycle (PgC yr^{-1}), $C_{\text{ppm\_to\_PgC}} = 2.123\ \frac{PgC}{ppm}$ is a conversion factor between partial atmospheric concentration of CO_2 and emitted Pg of carbon. A_{oc} is the ocean area (in m^2). $f_{a,s}$ is the transfer rate between ocean and atmosphere (in ppm $yr^{-1}\ m^{-2}$), represented as a function of the atmospheric and ocean carbon partial pressures:

$$f_{a,s} = k_g \cdot [\delta pCO_{2,a} - \delta pCO_{2,s}], \tag{2}$$

Where k_g is the gas exchange coefficient ($k_g = \frac{1}{9.06 \cdot A_{oc}} \text{yr}^{-1}\text{m}^{-2}$) and $\delta pCO_{2,s}$ is the partial pressure of the slab ocean, itself calculated as a function of the ocean temperature (T) and the carbon content of the mixed layer $(\delta \Sigma CO_2(t))$.

$$\delta pCO_{(2,s)} = F(\delta \Sigma CO_2(t), \text{T}) \tag{3}$$

F is the polynomial approximation given in equation 6b) of (Joos et al., 1996). Though this equation could include temperature feedback to the carbon cycle, the CICERO-SCM does not currently include this, implementing instead a static T= 18.2°C giving

$$F(x) = 1.3021x + 3.7929 \cdot 10^{-3}x^2 + 9.1193 \cdot 10^{-6}x^3 + 1.488 \cdot 10^{-8}x^4 + 1.2425 \cdot 10^{-10}x^5 \tag{4}$$

$\delta \Sigma CO_2$ is calculated as a historical integral of past air-sea fluxes $f_{a,s}$ modulated by a decay function r_s which represents transfer of carbon from the mixed layer to an (infinite) deep ocean sink.

$$\delta \Sigma CO_2(t) = \frac{c_{conv}}{h} \int_{t_o}^{t} f_{a,s}(t') r_s(t - t') dt' \tag{5}$$

Where h is the height of the mixing layer in meters, $c_{conv} = 1.722 10^{17} \frac{\mu mol \cdot m^3}{ppm \cdot kg}$ is a conversion factor from the flux from ppm to μmol and sea water from volume (m³) to mass (kg). The function r_s is defined by two empirical decay functions, the first for a period of less than two years, with a second empirical formulation for periods of two years or greater:

$$r_s \begin{cases} = 0.12935 + 0.21898 \cdot e^{-\frac{t}{0.034569}} + 0.17003 \cdot e^{-\frac{t}{0.26936}} + 0.24071 \cdot e^{-\frac{t}{0.96083}} \\ \quad + 0.24093 \cdot e^{-\frac{t}{4.9792}} \qquad\qquad\qquad\qquad\qquad \text{if } \mathbf{t < 2.0} \\ = 0.022936 + 0.24278 \cdot e^{-\frac{t}{1.2679}} + 0.13963 \cdot e^{-\frac{t}{5.2528}} + 0.089318 \cdot e^{-\frac{t}{18.601}} \\ \quad + 0.03782 \cdot e^{-\frac{t}{68.736}} + 0.035549 \qquad\qquad\qquad \text{if } \mathbf{t \geq 2.0} \end{cases} \tag{6}$$

where t is measured in years.

Different versions of both r_s and the biotic decay function r_b, described below and with standard form according to equation (8) can be sent by sending a function as input when defining the *concentrations_emissions_handler* object according to Table 1.

The CICERO-SCM also includes the impacts of the terrestrial ecosystem, including CO_2 fertilization and subsequent impact on decay of biospheric material (Joos and Bruno, 1996). Net primary productivity is described as a function of the atmospheric CO_2 concentration, which modifies the emissions timeseries directly according to equation (1).

The carbon uptake of the terrestrial cycle f_{fer} is represented as:

$$f_{fer}(t) = \delta f_{npp}(t) + \int_{-\infty}^{t} \delta f_{npp}(t') r_b(t - t') dt', \tag{7}$$

Where δf_{npp} (t) is the instantaneous Net Primary Productivity (NPP) from the current CO_2 concentration (in units of PgC per year = PgC per year) and r_b is an impulse-response function which represents the decay of the historically fertilized material produced during previous timesteps:

$$r_b = 0.70211 \cdot e^{-0.35t} + 13.4141 \cdot 10^{-3} \cdot e^{-\frac{t}{20.0}} - 0.71846 \cdot e^{-\frac{55t}{120.0}} + 2.9323 \cdot 10^{-3} \cdot e^{-\frac{t}{100.0}} \tag{8}$$

The various terms represent the decay of ground vegetation, wood, detritus and soil organic carbon, and time t is measured in years. $\delta f_{npp}(t)$ is represented as a function of the atmospheric CO_2 concentrations:

$$\delta f_{npp}(t) = f_{npp}\, \beta_f \ln\left(\frac{CO_{2,a}(t)}{278\text{ppm}}\right), \tag{9}$$

Where f_{npp} is a measure of global terrestrial NPP (here taken as 60PgC yr^{-1} (Atjay et al., 1979; Joos and Bruno, 1996), $CO_{2,a}(t)$ is the atmospheric concentration of CO_2 measured in ppm. β_f (beta_f in the model and Table 2) is the 'fertilization factor'.
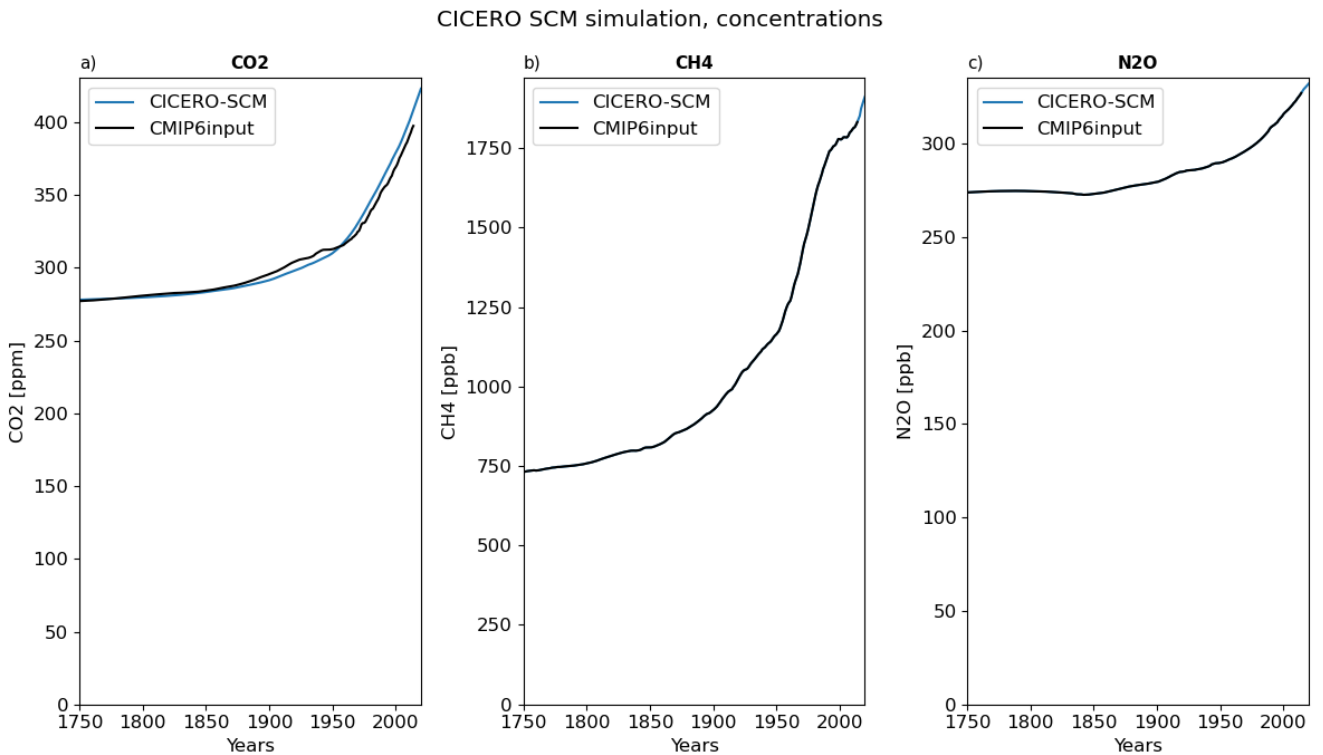
Figure 2: Calculated concentration of CO_2, CH_4 and N_2O from the CICERO-SCM from CMIP6 emissions time series (Meinshausen et al., 2017) compared to the concentrations of these gases prepared for CMIP6 (black line) from the same emissions inputs (Meinshausen et al., 2017). Note that the natural emissions of CH_4 and N_2O are adjusted so that the calculated concentrations match the observational based concentrations prepared for CMIP6.

Figure 2a shows the calculated concentrations of CO_2 from the CICERO-SCM using CO_2 emissions from (Meinshausen et al., 2017, 2020). For reference, the CO_2 emissions in 2014 split into 9.7 Pg carbon of fossil fuel emissions and 1.1 Pg carbon of landuse change emissions.

2.1.2 Non-CO₂ components concentration calculations

The atmospheric concentration of non-CO_2 gases is determined by a mass balance equation:

$$\frac{dC}{dt} = P - Q \cdot C = \frac{E}{\beta_{gas}} - C \cdot \frac{1}{\tau_{gas}} \tag{10}$$

where C is the concentration or mixing ratio of the gas (ppm, ppb), P is the production rate and Q is the loss rate. The production, P, is given by the emissions per year, E, converted to mixing ratio units with β_{gas}, τ_{gas} is the lifetime (in years). β_{gas} (BETA) and τ_{gas} (TAU1) are both gas specific constants read from the gaspam_file (see Table 3). The production (emissions) is a function of time t (in years), E=E(t), while the loss rate (Q) is assumed to be constant, except for the case of CH_4 (see section 2.1.3).

To solve this equation numerically, we use a first-order exponential integrator method. We first rearrange the equation as

$$\frac{dC(t)}{dt} + C(t) \cdot \frac{1}{\tau_{gas}} = \frac{E(t)}{\beta_{gas}}, \tag{11}$$

multiply both sides by $\exp\left(\frac{t}{\tau_{gas}}\right)$ and combine:

$$\frac{d}{dt}\left(C(t) \cdot \exp\left(\frac{t}{\tau_{gas}}\right)\right) = \frac{E(t)}{\beta_{gas}} \cdot \exp\left(\frac{t}{\tau_{gas}}\right) \tag{12}$$

The emissions (E) and mixing ratios (C) are annual, and we assume that over each one-year period they are constant. This means that we can solve the equation exactly for each time step, t to $t + \Delta t$, where $\Delta t = 1$ as the data is annualized. First, integrate both sides of the equation from t to t+1, noting that E(t) is constant between t+1 and t:

$$C(t+1) \cdot \exp\left(\frac{t+1}{\tau_{gas}}\right) - C(t) \cdot \exp\left(\frac{t}{\tau_{gas}}\right) = \frac{E(t)\tau_{gas}}{\beta_{gas}} \cdot \left[\exp\left(\frac{t+1}{\tau_{gas}}\right) - \exp\left(\frac{t}{\tau_{gas}}\right)\right] \tag{13}$$

Then multiply both sides by $\exp\left(-\frac{t+1}{\tau_{gas}}\right)$, noting that $\exp\left(-\frac{t+1}{\tau_{gas}}\right) \cdot \exp\left(\frac{t}{\tau_{gas}}\right) = \exp\left(-\frac{1}{\tau_{gas}}\right)$), leads to

$$C(t+1) = C(t)\exp\left(-\frac{1}{\tau_{gas}}\right) + \frac{E(t)\tau_{gas}}{\beta_{gas}} \cdot \left[1 - \exp\left(-\frac{1}{\tau_{gas}}\right)\right] \tag{14}$$

This implementation is appropriate for discrete input data only, where the emissions (and concentrations) are assumed constant throughout the year. For a timestep of less than one year, the emissions (E) and mixing ratio (C) would need to have

a resolution of less than one year to match the time step. If working with emissions not assumed static over the sub yearly timescale, the original equation would be solved either analytically or using a numerical solution to the original differential equation (Aamaas et al., 2013). This version of the model only works for yearly data that follows this assumption.

Given this assumption, the method outlined here is an exact solution, for each time step, utilizing the fact that emissions are constant in each time step. The solution can also be interpreted in terms of production and loss. The first term on the right-hand side represents the mixing ratio at the start of the time-period (C_t), which decays according to the loss rate over one year. The second term on the right-hand side represents the emissions added in that year (E_t), which are assumed constant, and thus accumulate as sustained emissions over the year (Aamaas et al., 2013). At the end of the time-period, C_{t+1}, the mixing ratio is thus the contribution from material already in the atmosphere (first term) plus the contribution from material added to the atmosphere over the year (second term).

Several simplifications can help explain equation (14) and the unique characteristics of different non-CO_2 components. For a long-lived species, where $\tau \gg 1$, such as N_2O, then the exponential term is close to one, and $C_{t+1} \approx C_t + \Delta$, where Δ is a small contribution from new emissions. For a short-lived species, where $\tau \ll 1$, such as sulfur dioxide (SO_2), then the exponential term is close to zero, and $C(t) \approx E(t) \cdot \frac{\tau_{gas}}{\beta_{gas}}$, showing that the mixing ratio is approximately a linear scaling of the emissions. And in fact, for SO_2 and other aerosols, such a direct emissions scaling is used to obtain forcing directly from emissions with no separate calculation of concentrations.

2.1.3 CH$_4$ - emissions to concentrations

The atmospheric concentration of CH_4 is determined by the mass balance equation (equation 14), leading to the solution and treatment as described above in section 2.1.2. But for CH_4, the lifetime τ is not necessarily constant. The total lifetime is a combination of the lifetime with respect to OH (τ_{OH}), stratospheric lifetime (τ_{strat}) representing the chemical losses in stratosphere, and soil lifetime (τ_{soil}) representing the soil loss. The total lifetime and the individual lifetimes are related by: $\frac{1}{\tau} = \frac{1}{\tau_{OH}} + \frac{1}{\tau_{soil}} + \frac{1}{\tau_{strat}}$. The values of β_{CH_4} (BETA), τ_{OH} (TAU1), τ_{soil} (TAU2), τ_{strat} (TAU3) are specified in the gaspam_file (Table 3) with default values of 2.78 Tg CH_4 ppbv^{-1}, 9.6 years, 120 years, and 160 years (Ehhalt et al., 2001), used. The total lifetime of CH_4 is 8.4 years.

The lifetime of CH_4 due to OH depends both on the CH_4 itself and emissions of NO_x, CO and NMVOCs. CH_4 influences its own lifetime since the reaction between CH_4 and OH also is a significant loss reaction for OH. Increased emissions and higher atmospheric levels of CH_4 thus decrease the levels of OH. This will increase the chemical lifetime of CH_4, thereby further increasing the atmospheric levels of CH_4. CO and NMVOCs also have OH as a main loss reaction, and increased emissions of these components will decrease the levels of OH and increase the lifetime of CH_4. Enhanced levels of NO_x will work in the opposite direction, as NO_x acts as a source of OH. Enhanced NO_x will increase OH and decrease the CH_4 levels. Several parameterization options are available in the CICERO-SCM to deal with these effects on the CH_4 lifetime. The "lifetime_mode" can be set to the following in the pamset_emiconc (Table 2):

"TAR" (default) where the τ_{OH} is adjusted following (Ehhalt et al., 2001) (Table 4.11 footnote b). $\frac{1}{\tau} = q = q \cdot$ (d $\ln C_{OH} + 1$), where

$$d \ln C_{OH} = -0.32 \cdot \{\ln[C_{CH_4}(yr)] - \ln[1751.0]\} + 0.0042 \cdot [E_{NO_x}(yr) - E_{NO_x}(2000)] + 0.000105$$
$$\cdot [E_{CO}(yr) - E_{CO}(2000)] - 0.000315 \cdot [E_{NMVOC}(yr) - E_{NMVOC}(2000)],$$

"WIGLEY" , where $\tau_{OH} = \tau_{OH}^0 \cdot \left(\frac{C}{C_0}\right)^N$ where C is the CH$_4$ concentration, C_0 is a reference CH$_4$ concentration of 1700 ppb and the exponent N is 0.238 (Osborn and Wigley, 1994).

"CONSTANT_12" where $\tau_{OH} = 12.0$

If some other string is sent for this parameter, a flat lifetime from the *gaspam_file* is used. This flexibility in OH lifetime options can allow the user to explore hypothesis, and also allows for the user to add and adapt a new OH lifetime scheme in a separate fork of the code without much effort.

There are also natural emissions of CH$_4$ which maintain a CH$_4$ concentration in the atmosphere in the absence of anthropogenic emissions (Saunois et al., 2020). To accurately represent the observed concentration, natural emissions of CH$_4$ can be precalculated (*precalculate_natural_emissions.py* in scripts/prescripts subfolder) with the same set up (lifetime mode and anthropogenic emissions) and these are added to E(t) before the calculation in eq. 14. Further details on this can be found in Appendix B on natural emissions of CH$_4$ and N$_2$O. Precalculated natural emissions time series can be specified as an input file or input dataset (see Table 1). The model can also be run with fixed natural emissions specified in the gaspam_file (Table 3), and this is the model behavior when no data or files with natural emissions are sent and can also be used to provide constant natural emissions for other chemical components.

With the adjusted historical natural emissions of CH$_4$, the calculated CH$_4$ concentrations by design match observations of CH$_4$ concentration (Fig. 2b). The model can also be run with fixed natural emissions specified in the gaspam_file (Table 3) and then the calculated concentration will give rise to discrepancies compared to observations, due to the large uncertainties in the CH$_4$ budget terms (Saunois et al., 2020).

2.1.4 N$_2$O - emissions to concentrations

The atmospheric concentration of N$_2$O is determined by the same mass balance equation (equation 14) as for CH$_4$, but with a single constant lifetime of 109 years (Smith et al., 2021b), specified in the *gaspam_file* (Table 3). The parameter β_{N_2O} (BETA) is given as 4.81 Tg[N] ppbv^{-1}, and hence the emission input to the model is given in Tg[N].

As for CH$_4$, the natural emissions can either be kept fixed with a value prescribed in the *gaspam_file* or sent as a precalculated file or dataset so that total (natural and anthropogenic) emissions timeseries and the model setup will reproduce the historical concentration (Fig. 3c). For more on how natural emissions are estimated including assumptions for the future, see Appendix B on natural emissions of CH$_4$ and N$_2$O.

2.1.5 CO_2, CH_4 and N_2O – concentrations to forcing

Based on the calculated concentrations, radiative forcing for CO_2, CH_4 and N_2O is calculated based on the simplified

300 expressions in Table 1 of (Etminan et al., 2016) that accounts for the overlap between the three components. The equations in (Etminan et al., 2016) represent the radiative forcing that include adjustment to stratospheric temperatures (SARF). The initial concentrations of CO_2, CH_4 and N_2O used for the calculations are the concentration in the nystart year from the input file.

305 To include additional tropospheric adjustments, an adjustment factor can be specified in the *gaspam_file* (Table 3) to convert from SARF to Effective Radiative Forcing (ERF) for each of the components. The default values in Table 3 are taken from AR6 and the additional adjustments will increase the radiative forcing by 5% for CO_2, decrease it by 14% for CH_4 and increasing it by 7% for N_2O (Forster et al., 2021).

310 The calculated CO_2 ERF is less than the ERF timeseries from IPCC AR6 (Forster et al., 2021) based on observed concentrations before 1950, and larger after 1950 (Fig. 3a). The reason for this is the under and overestimation of the CO_2 concentration (Fig. 2a) and that 2xCO2ERF, that is the effective forcing strength of a doubling of CO_2, based on (Etminan et al., 2016) is stronger than the 2xCO2ERF in AR6 based on (Meinshausen et al., 2020). The CH_4 ERF in Fig. 3b shows a reasonably good match. The N_2O ERF timeseries is in the lower range compared to the timeseries presented in IPCC AR6

315 (Forster et al., 2021). The difference can be explained by assuming a different pre-industrial concentration value in the run, and by the fact that (Forster et al., 2021) uses simplified expression as used in (Meinshausen et al., 2020) rather than the expressions from (Etminan et al., 2016) used in CICERO-SCM.

CICERO-SCM simulation, Radiative Forcing
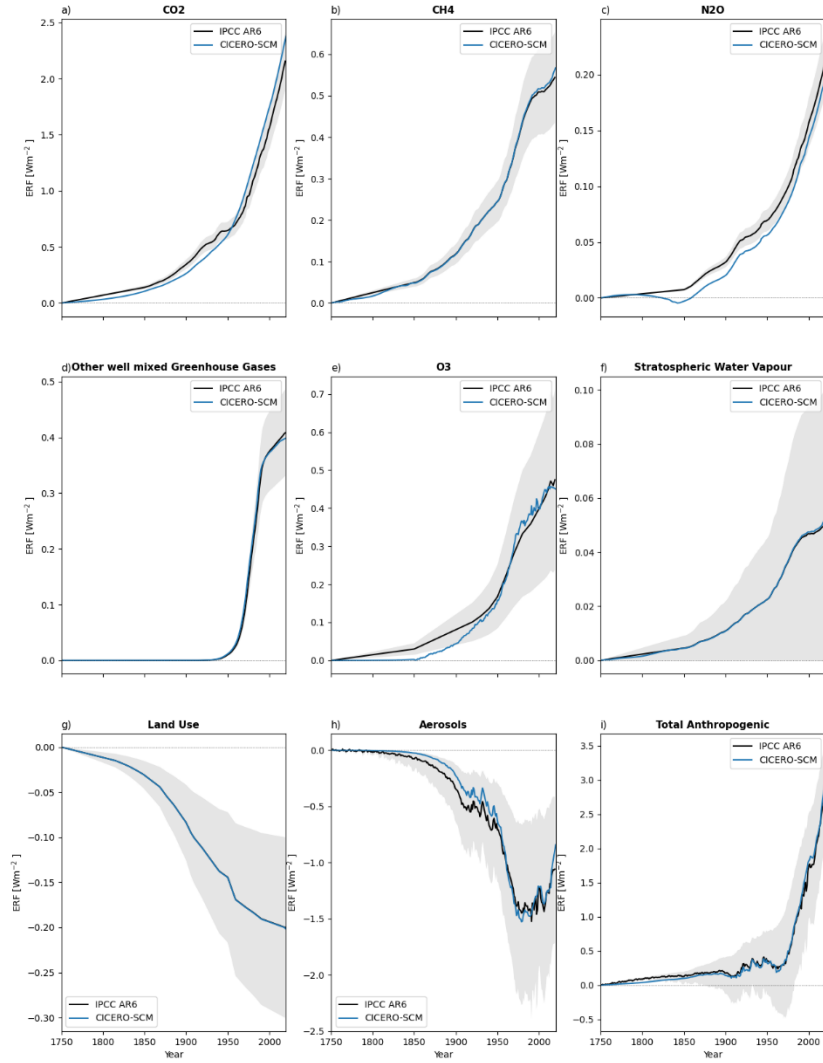
Figure 3: Calculated ERF from CICERO-SCM for selected components from 1750 to 2020. For comparison, the ERF timeseries from IPCC and uncertainty ranges from this same dataset are also shown (Smith et al., 2021a, b). a) for CO₂, b) CH₄, c) N₂O d) other well mixed GHGs that is the sum of contribution from CFC-11, CFC-12, CFC-113, CFC-114, CFC-115, CHBr, CCl4, CH3CCl3, HCFC-22, HCFC-141b, HCFC-142b, C2F6, C6F14, CF4, SF6, HCFC-123, H-1211, H-1301, H-2402, HFC125, HFC134a, HFC143a, HFC227ea, HFC23, HFC245fa, HFC32 and HFC4310mee e) total O₃, sum of tropospheric and stratospheric O₃, f) stratospheric water vapor, g) land use (note that the CICERO-SCM uses the IPCC ERF timeseries as input), h) total aerosol ERF and i) Total anthropogenic forcing. Note the different scales on the y-axis. Beyond 2014 the ssp245 future projections have been used as inputs.

2.1.6 Effective radiative forcing for other long lived greenhouse gases

For the other long lived or medium lifetime greenhouse gases (CFCs, HFCs, HCFCs), the atmospheric concentrations are calculated based on the mass balance equation, emission time series, BETA values and a single lifetime both specified in the *gaspam_file* (Table 3) as described in section 2.1.2. The lifetimes are as in IPCC (7.SM.7 in (Smith et al., 2021b)).

For these components radiative forcing is calculated based on a radiative efficiency (Table 7.SM.7 in (Smith et al., 2021b):

$$SARF = ALPHA \cdot (C - C_0) \tag{15}$$

Where ALPHA is read from the *gaspam_file* (Table 3), C is the concentration and C_0 the concentration in the *nystart* year. As most of these components are of anthropogenic origin, C_0 will be zero when starting from pre-industrial. Some components, however, have natural background concentrations. The pre-industrial concentrations are provided in the concentration file and natural emissions are expected to be included for each year in the emission file, otherwise a flat natural emission component can be specified in the *gaspam_file*.

Each component also has an option to include a conversion from SARF to ERF (ERF = SARF_TO_ERF $\cdot$ SARF), to get the ERF that will be output and passed to the *upwelling_diffusion_model.py*.

In (Forster et al., 2021) CFC11 and CFC12 have SARF to ERF adjustment factors of 13 and 12 % respectively. All other components have SARF to ERF factors of 1. However, different SARF to ERF conversion factors can be specified in the gaspam_file (see Table 3).

The calculated ERFs for the other GHGs compare well with IPCC AR6 timeseries (Fig. 3d).

2.1.7 Tropospheric O_3

The tropospheric O_3 forcing is specified in the *pamset_emiconc* as qo3 (Table 2), that is the radiative forcing in the reference year (ref_year) specified in the same parameter set. The default values are 0.5 Wm^{-2} in ref_year 2010, based on (Smith et al., 2021b). The qo3 can include adjustments and be treated as ERF, or a factor converting SARF to ERF can be included in the *gaspam_file* (Table 3).

The time series of tropospheric O_3 forcing is calculated by combining the concentrations of CH_4 and emissions of NOx, CO and NMVOC following (Table 4.11 footnote b of (Ehhalt et al., 2001))

Assuming a tropospheric O_3 burden of 30 DU (Dobson Units) in the reference year, the tropospheric O_3 burden is calculated as:

$$C_{O_3}(t) = 30.0 + 6.7 \cdot \{\ln[C_{CH_4}(t)] - \ln[C_{CH_4}(t_{ref})]\} + 0.17 \cdot [E_{NO_x}(t) - E_{NO_x}(t_{ref})] +$$
$$0.0014 \cdot [E_{CO}(t) - E_{CO}(t_{ref})] + 0.0042 \cdot [E_{NMVOC}(t) - E_{NMVOC}(t_{ref})] \tag{16}$$

where C-terms denote concentrations, E-terms are emissions, t is time in years and is t_{ref} is the reference year, the default value for this is 2010.

The radiative forcing is calculated by scaling the qo3 (tropospheric ozone SARF in the reference year in W m^{-2}) by changes in O$_3$ burden:

$$SARF = qo3 \cdot \frac{C_{O_3}(t) - C_{O_3}(t_{emstart})}{C_{O_3}(t_{ref}) - C_{O_3}(t_{emstart})} \tag{17}$$

where $t_{emstart}$ is the year when running with everything from emissions start.

Before emissions start, the forcing is scaled by fossil fuel CO$_2$ emissions and t_0 is the first year of the run, i.e. nystart.

$$SARF = qo3 \cdot \frac{E_{CO_2FF}(t) - E_{CO_2FF}(t_0)}{E_{CO_2FF}(t_{ref}) - E_{CO_2FF}(t_0)} \tag{18}$$

Tropospheric O$_3$ is a short-lived component, and the global forcing is split into hemispheric forcing. The hemispheric weights for the global forcing is taken from the multimodel results in (Skeie et al., 2020) and is 1.45 for the Northern Hemisphere and 0.55 for the Southern Hemisphere as implemented in the routine *calculate_hemispheric_forcing*. The total O$_3$ forcing (tropospheric and stratospheric) is shown in Fig. 3d, and tropospheric O$_3$ ERF alone is shown in Fig. S8.

2.1.8 Stratospheric O$_3$

Loss of stratospheric O$_3$ is calculated from the concentration of chlorine and bromine containing components three years prior to the year in question to account for transport from the troposphere to the stratosphere, and scaled by the number of chlorine or bromine atoms they contain:

$$SARF = -\frac{0.287737}{1000.0} \cdot \left[0.000552 \cdot \sum_i \left(N_{Cl_i} \cdot C_{Cl_i}(t-3) \right)^{1.7} + 3.048 \cdot \sum_j N_{Br_j} \cdot C_{Br_j}(t-3) \right] \tag{19}$$

where the sums run over the chlorine and bromine containing components respectively, the C-terms are concentrations (pptv) of each of these, and the N-terms are the numbers of chlorine or bromine atoms in each of them, t is the time in years. The functional form is based on Appendix 2 of (Harvey et al., 1997) and the scaling has been updated in line with (Forster et al., 2007). This has been generalized a bit from the Fortran version, where the exact chlorine and bromine components considered were hard coded, rather than identified from the substances contained in the gaspam_file (Table 3).

The total O$_3$ ERF (tropospheric plus stratospheric) is shown in Fig. 3e and stratospheric O$_3$ separately in Fig. S8.

2.1.9 Stratospheric water vapour

CH$_4$ oxidized in the stratosphere produces water vapour. In the dry stratosphere, this additional water vapour will cause additional radiative forcing. The CH$_4$ induced stratospheric water vapor ERF is calculated by scaling the CH$_4$ ERF by a factor *qh2o_ch4* specified in the *pam_emiconc* parameter set. The default value is 0.092, that is 9.2 % of the CH$_4$ forcing in the reference year (Forster et al., 2021; Winterstein et al., 2019). The ERF timeseries for stratospheric water vapour is shown in Fig. 3f.

2.1.10 Albedo from land use change

The historical surface albedo land-use change forcing used in the model is a prescribed forcing timeseries. The default time series used in the model is from IPCC AR6 (Forster et al., 2021; Smith et al., 2021b) and extended for RCMIP (Nicholls et al., 2021, 2020). ERF timeseries of this is show in Fig. 3g, beyond 2014, the albedo forcing projections for ssp245 are used.
390 The hemispheric split of forcing is based on the multi model results from (Smith et al., 2020) and implemented in the routine *calculate_hemispheric_forcing*.

2.1.11 Aerosol effective radiative forcing

The ERF for aerosol radiation interaction *(ERFari)* of sulfate, fossil fuel and biofuel (FFBF) black carbon (BC), organic carbon (OC) and biomass burning (BMB) aerosols are included in CICERO-SCM, and the aerosol forcing in *ref_year* (t_{ref})
395 for each aerosol component is specified in the pamset_emiconc (Table 2). The *ERFari* values in *ref_yr* are scaled by corresponding historical emissions of SO_2, BC FFBF, OC FFBF and biomass burning aerosols (BMB_AEROS).

The *ERFari* timeseries for individual aerosol components are shown in Fig. 4a. The total aerosol *ERFari* timeseries is shown in Fig. 4b and shows a good match with IPCC AR6 timeseries.

$$E_{ref} = E(t_{ref}) - E(t_0), \qquad \text{ERF} = q_{aer}\frac{E(t) - E(t_0)}{E_{ref}}, \qquad (20)$$

400

where *E(t)* is the emissions of each aerosol species at time *t* in years and q_{aer} is the forcing for this component in t_{ref} and is tunable parameter (see Table 2) for each component.

The net ERF from biomass burning aerosols (BMB_AEROS) is calculated using the input BMB_AEROS_OC as biomass burning emissions from OC and BC are assumed to be correlated and scaled according to equation 20 with the parameter
405 *qbmb*. The default value of this parameter is 0, so the user needs to set it to a different value to include the effects of biomass burning aerosols.

The ERF for aerosol cloud interaction (*ERFaci*) in *ref_year* is linearly scaled with SO_2 emissions, and calculated as *ERFari* according to equation (20), as studies indicate that the total global effect is linear with SO_2 (Kretzschmar et al., 2017). The aerosol forcing components from a default run of the CICERO-SCM are shown in Fig. 4a. The split in *ERFari* and *ERFaci*
410 timeseries are show in Fig. 4b and compared to the IPCC AR6 results (Forster et al., 2021). ERFari follows the AR6 results quite closely, while ERFaci are not as close to the AR6 mean, however, the uncertainty range for this is very large.

The hemispheric split of aerosol forcing is based on multi-model results from (Smith et al., 2020) and implemented in the routine *calculate_hemispheric_forcing*.

CICERO-SCM simulation, Aerosol Radiative Forcing
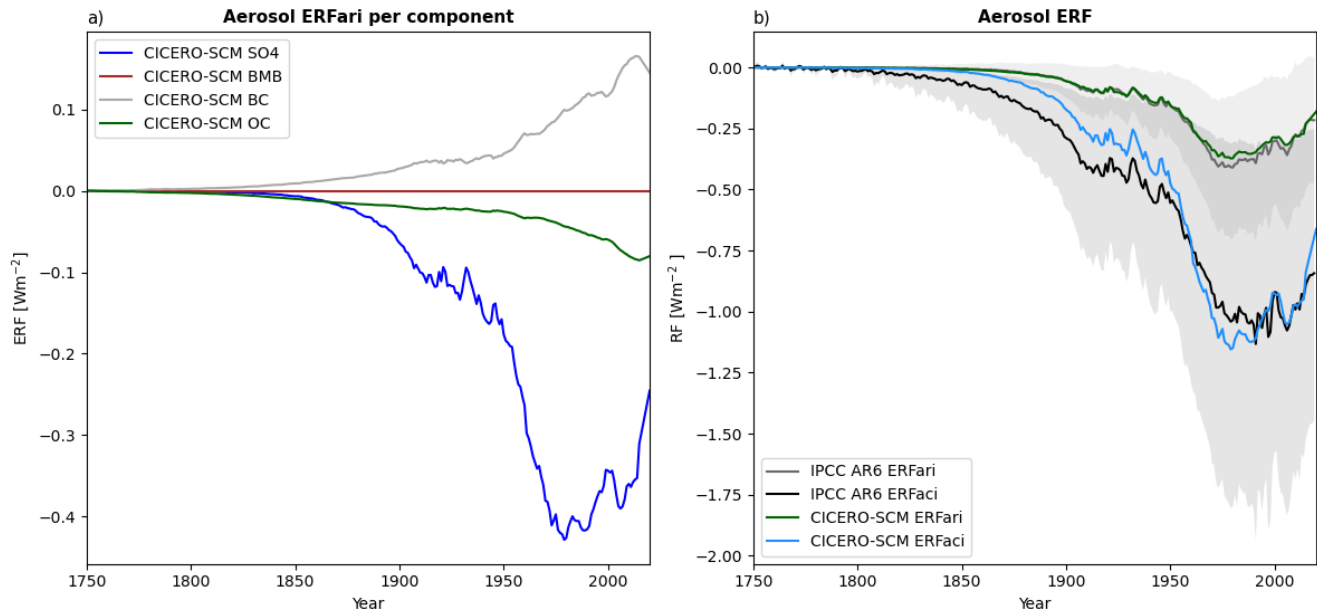
415

Figure 4: Part a shows aerosol radiation interaction forcing per aerosol component, and part b shows aerosol cloud interaction and sum of aerosol radiation interactions for all the components compared to AR6 results (Forster et al., 2021).

2.1.12 Solar and volcanic forcing

420   Solar forcing and volcanic forcing can be added as input time series. If the *sunvolc* parameter is set to 1, the model will either use user defined files or datasets or use default files. Volcanic forcing series can be defined differently in each of the hemispheres, and even with monthly time resolution. Figure 5 shows default input timeseries of solar and volcanic forcing. These defaults are taken from (Nicholls et al., 2021, 2020), however, for values beyond year 2015 the following approximation has been made; solar forcing is assumed to be zero, whereas volcanic forcing is set to the mean forcing value
425   in years 2006-2015.
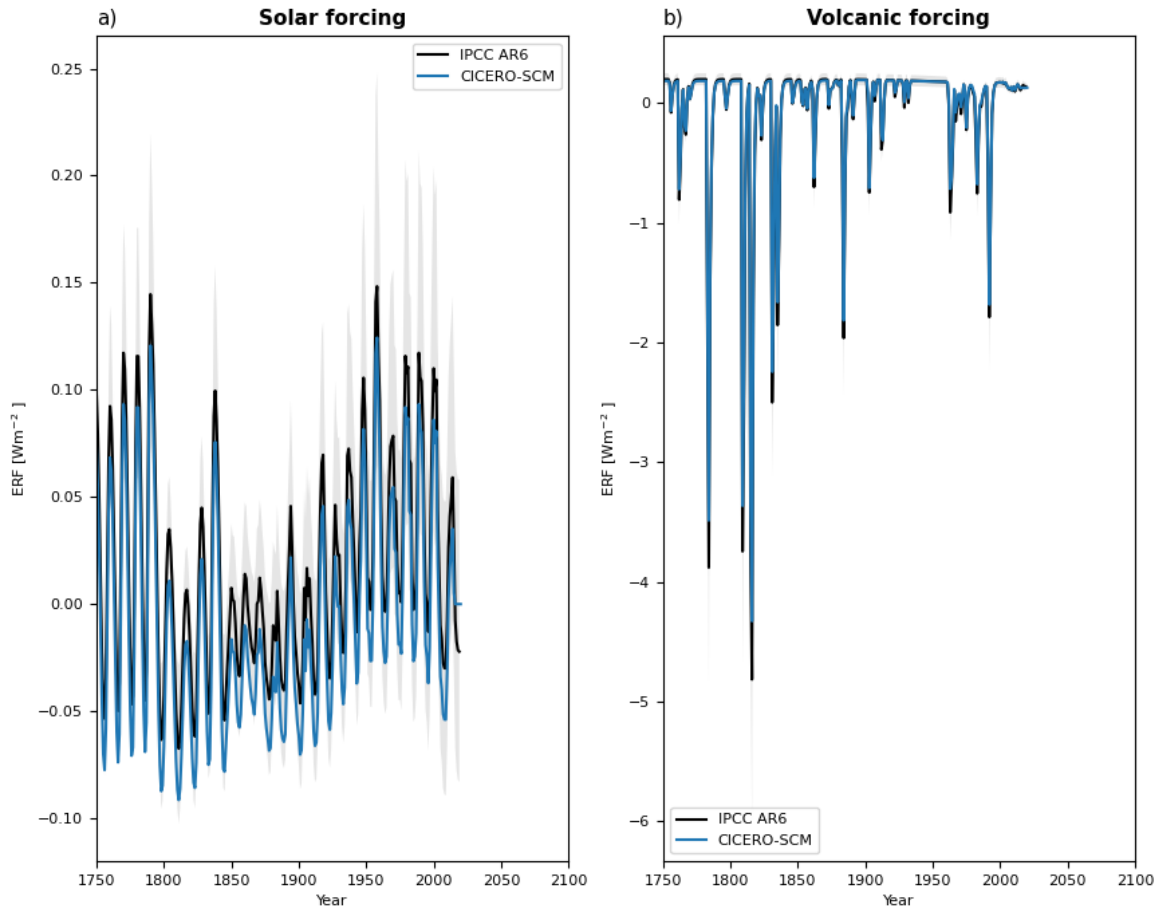
Figure 5: Default natural ERF timeseries for solar forcing (a) and volcanic forcing (b) used in the CICERO-SCM taken from RCMIP (Nicholls et al., 2021, 2020) compared to AR6 results (Forster et al., 2021; Smith et al., 2021b).

430 **2.1.13 Perturbing forcing or emissions timeseries**

A common application of SCMs is to isolate and quantify the contributions to global radiative forcing and temperature change over time from individual anthropogenic emissions or sources, such as economic sectors. While there are different approached to such attribution (e.g. (Boucher et al., 2021; Grewe, 2013)), a well-established method is to have a perturbed case where the emissions of interest are subtracted from a baseline case that includes all emissions. The attribution is thus the

435 difference between the baseline case and the perturbed case (den Elzen et al., 2005; Fuglestvedt et al., 2008).

The CICERO SCM includes built-in options that enable this type of simulation, baseline and perturbation. Specifically, two additional files can be input to the run, one that that gives emission trajectories to be subtracted and one that gives the radiative forcing to be subtracted. The former is used in the case of the well-mixed greenhouse gases, while the radiative forcing perturbations are applied for the short-lived climate forcers.

440 In some cases, a given sector may affect climate through radiative forcing mechanisms that are not included in the SCM. A notable example is the formation of contrail-cirrus from aviation emissions. It is possible to also include such ERF perturbations, which are then grouped in a category "OTHER" and subtracted from the total net RF at the end of the concentrations-to-forcing step of the model flow.

The time series of emissions and ERF to be extracted must be pre-defined in a specific format (sample files provided in the
445 open-source code base). If not directly available from more complex models, ERF time series are commonly derived by scaling best-estimate present-day radiative efficiencies (i.e., ERF per unit emission) by available historical and/or future emissions trajectories. For examples of how this has previously been done, including more chemically complex climate drivers such as NOx-induced changes in O_3 and CH_4, see e.g. (Skeie et al., 2009)

2.2 Upwelling diffusion/ energy balance model

450 To calculate temperature change and storage of heat in the ocean as a response to the radiative forcing, an energy balance/upwelling diffusion model is used. The model is the hemispheric version (Schlesinger et al., 1992) of the global energy balance/upwelling diffusion model described in (Schlesinger and Jiang, 1990), and the structure of the model is shown in Fig. 6.

For each hemisphere the ocean is subdivided into 40 vertical layers where the uppermost ocean layer is the mixed layer. The
455 ocean also has a polar region, where heat is transported from the mixed layer into the deep ocean representing deep water formation, i.e. sinking of cold water masses with relatively high salinity. Figure 6 shows the schematic ocean in the model.

The model is forced by hemispheric radiative forcing and the climate response is governed by climate sensitivity, which is an explicit parameter in the model that takes the feedback processes in the climate system into account. The climate sensitivity
460 parameter, λ (lambda), is the equilibrium climate sensitivity (defined as the equilibrium temperature response following a doubling of the CO_2 concentration) divided by the radiative forcing of a doubling of CO_2. Based on the formula in (Etminan et al., 2016), SARF is 3.8 W m^{-2} for a CO_2 doubling, and taking into account the adjustments of 5% (Forster et al., 2021) the 2xCO2 ERF is 4.0 W m^{-2}.

465 In each hemisphere heat is exchanged between the atmosphere and the ocean in the upper mixed layer of the ocean. Heat is exchanged between each layer and the layers next to it via both diffusion and vertical upwelling advection, and horizontally through interhemispheric heat exchange. Heat is also transported into the polar ocean in the mixed layer, and back into the main ocean in the bottom most layer. This leads to a set of coupled differential equations which are solved by a mix of

forward and backward implicit calculations, to find the temperature change in each ocean layer. Equations are taken and
470   implemented according to appendix B of (Schlesinger et al., 1992), and the strengths of the various processes are defined by
parameters listed in Table 4, and the equations and their implementations are also detailed in Appendix C.
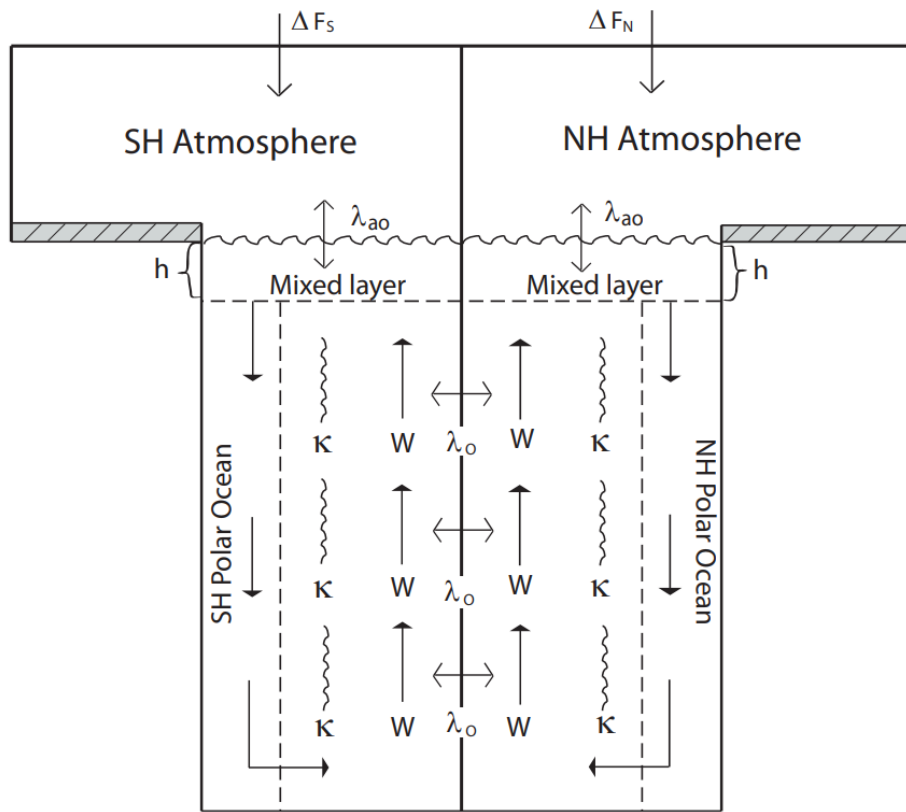
Figure 6: Redrawn from (Schlesinger et al., 1992). The difference in ocean and land fraction between northern and southern hemisphere is considered in the model, but not illustrated in the figure.

475

Parameter	Default value	Unit	Description and range*
Rlamdo	15.0	W m^{-2} K^{-1}	Air-sea heat exchange parameter, λ_{ao} in Fig. 6, range 5-25
Akapa	0.66	cm^2 s^{-1}	Vertical heat diffusivity, κ in Fig. 6, range 0.06-0.8
Cpi	0.21	unitless	Polar parameter, scale between polar and non-polar temperatures, range 0.161-0.569
W	2.2	m yr^{-1}	Vertical velocity, upwelling rate, W in Fig. 6, range 0.55-6 When threshtemp is not zero, the vertical velocity is effectively lower than this.

Beto	6.9	W m^{-2} K^{-1}	Oceanic interhemispheric heat exchange coefficient, λ_o in Fig. 6, range 0-7
Threstemp	7.0	unitless	Scales vertical velocity (W) as a function of mixed layer temperature, not shown in Fig. 6. Set to 0 if you don't want to include this parameter. Default is a 30% drop in vertical velocity at 7 K increase in mixed layer temperature.
Lambda	0.61	K W^{-1} m^{-2}	Equilibrium climate sensitivity divided by 2xCO2 radiative forcing (4.00 W m^{-2}), i.e. λ. Calibration range 0.5-1.25
Mixed	107	m	Mixed layer depth, h in Fig. 6, range 25-125
Foan	0.61	unitless	Fraction of Northern Hemisphere covered by ocean
Foas	0.81	unitless	Fraction of Southern Hemisphere covered by ocean
Ebbeta	0.0		Atmospheric interhemispheric heat exchange, not normally used and not shown in Fig. 6, but equations including this parameter are included in the code
Fnso	0.7531	unitless	Ratio between ocean areas in Northern and Southern Hemispheres, should equal foan/foas
Lm	40	unitless	Number of vertical layers of the ocean, including the mixed layer.

Table 4: pamset_udm. Parameters in the Energy Balance/Upwelling diffusion model, default values and possible ranges. *Ranges taken from (Aldrin et al., 2012) except the ranges for W and lambda which are as used in the calibration run proof-of-concept.

In addition to what is included in the (Schlesinger et al., 1992), the CICERO-SCM includes a *threstemp* parameter, which

480   changes the upwelling advection velocity depending on temperature according to (Raper et al., 2001). The parameter

threstemp is the temperature when the upwelling velocity is reduced by 30%. With *threstemp* equal to 0, *W* will be constant,

and is a way of omitting upwelling velocity dependency on temperature. Otherwise, the way this parameter is scaled means

that when $\Delta T = 10/3*threstemp$ the advection will stop completely, and if the temperature surpasses this, that advection

speed will become negative.

485

The temperature changes in the ocean layer calculated in the energy balance/upwelling diffusion model is finally used to

calculate values for the ocean heat content (OHC) and ocean heat content of the upper most 700 meters (OHC700). For each

hemisphere separately and as a global average of the two, it is used to calculate the three temperature quantities: T_{air}, that is

the global surface air temperature (GSAT), T_{sea}, the global sea surface temperature, and T_{blended}, the combined quantity

490   calculated from the mixed layer ocean temperature over the ocean and atmospheric temperature over land (GMST), Finally

hemispheric and global averages for the radiative imbalance (RIB) is obtained. All these quantities are derived from calculations of the temperature T_1 in the 40 layers of the ocean for each month of the year.

The temperature values are calculated from the ocean mixed layer temperature T_1 according to:

$$T_{\text{sea}} = \overline{T_1}, \qquad T_{\text{air}} = \overline{\frac{q + f_{\text{ocean}} \cdot \lambda_{ao} \cdot T_1}{\frac{1}{\lambda} + f_{\text{ocean}} \cdot \lambda_{ao}}}, \qquad T_{\text{blended}} = \overline{f_{\text{ocean}} \cdot T_{\text{sea}} + (1 - f_{\text{ocean}}) \cdot T_{\text{air}}}, \tag{21}$$

495   where means are taken over twelve sub-yearly timesteps, q is the mean forcing over the preceding year (in Wm^{-2}), f_{ocean} is the ocean fraction in the area under consideration (Northern Hemisphere, Southern Hemisphere or global), λ_{ao} and λ are the tunable parameters rlamdo and lambda respectively (see Table 4 for details and units) and T_1 is the temperature in uppermost ocean layer i.e. in the mixed layer.

500   The radiative imbalance (RIB) and ocean heat content (OHC) are similarly derived according to:

$$\text{RIB} = \text{ERF} - \frac{T_{\text{blended}}}{\lambda}, \qquad \text{OHC} = \sum_{l=1}^{\text{maxdepth}} \rho \cdot c_p \cdot A_{\text{Earth}} \cdot z_l \cdot T_l \cdot f_{\text{ocean}}, \tag{22}$$

where ρ is the density of seawater (assumed here to be constant at 1030 kg m^{-3}), c_p is the specific heat capacity of seawater $(3.997 \cdot 10^3 \frac{J}{\text{kg K}})$, A_{Earth} is the surface area of the earth (in m^2), z_l is the height of the layer in meters. The sum goes over all the layers of the ocean either down to 700 meters, in which case the last layer is only a fractional layer, or all the way down,

505   depending on whether the calculation is for OHC down to 700 meters, or for total OHC. In practice the ocean heat content in each hemisphere is added together for each layer in the sum, hence the area used, A_{Earth}, is rather the area of a hemisphere $(2.55 \cdot 10^{14} \text{ m}^2)$.

2.3 Model differences between new Python version and old FORTRAN version

510   The Python version is overall quite faithful to the previous FORTRAN version (at least it is possible to run it quite comparably). However, the Python version has more flexibility in what can be changed using parameters rather than what is hardcoded. For instance, the addition of SARF_TO_ERF parameters in the *gaspam_file* is a new addition, as is the option to run for different sets of years not starting in 1750, and many new tunable parameters have been added. In the FORTRAN version you could tune the parameters lambda, akapa, cpi, W, rlamdo, beto, mixed, qbmb, qdirso2, qindso2, qbc, qoc and

515   qo3 using a parameter file needed for every run. In the Python version you can also tune threstemp, qh2o_ch4 and beta_f. You can also change parameters like the reference year, the ocean fractions in each hemisphere (foan and foas). You can also choose and even tune the functional forms for the carbon mixed layer pulse response function (eq. 5) and the biotic decay function (eq. 8). With the Python version, swapping between emissions or concentrations driven runs or simply accessing functions from the code is much easier than it was in the FORTRAN version, where such changes required producing a new

520 compiled executable from a modified version of the code. Since the code is openly available and more readable, a user can also much more easily change some part of the code to make even more parameters tunable, or even swap out some of the modules, running for instance with a simplified energy balance model. In addition, the model can be run with both file input and dataset inputs, and functionality for reading from files or handling dataset inputs is separated from the main code.

The Python code is also fully open and can be included as a regular Python package using pip. It includes automatic tests

525 including regression test to make sure the results from the energy balance model can be directly comparable to the previous version, and the emissions to forcing part can be comparable enough (this part of the calculation includes quite a lot of subtractions of nearly equal numbers, which means the comparison is less direct between the two versions). The regression tests directly compare energy balance output from the FORTRAN version to check that given the same forcing input, temperatures and ocean heat content are the same up to a relative error less than 1% throughout the run for a few different

530 forcing scenarios (including a single year forcing change, a 1% increase in CO2 per year experiment and running with and without volcanic and solar forcing). The modelling flow from concentrations from to forcing and temperature is tested in a similar way using a typical historical run, but when going all the way from emissions, the beginning of the run involves small values calculated by subtracting numbers of very similar size from each other, meaning that rounding differences become important, hence we only require regression up to 1% for a couple of years for the test to pass.

535 The code also includes plotting capabilities, and tools for distribution runs and calibration which we will describe in further detail below. The automatic plots generated include time series plots of ocean heat content, radiative imbalance, temperature, and component separated plots for emissions, concentrations, and radiative forcing. Examples of these plots for a historical run using all default parameters are included in Appendix A.

With the publicly available Python version on GitHub, there are also various example scripts to show usage, as well as

540 scripts to prepare natural emission files for CH_4 and N_2O and perturbation files. Automatically generated documentation for the code, as well as a descriptive readme file to describe usage is also included.

Currently the code is somewhat slower than the original FORTRAN code was. A standard run from 1750 to 2100 from emissions to concentrations with the FORTRAN version usually takes under half a second, whereas the updated code takes around three seconds to do the same. This is a point for future improvement; however, the readability is considerably

545 improved.

Figure 7 shows how temperature output from the same parameter distributions used in the AR6 process results compares when run in the new version and the original FORTRAN version. Both the new Python version, and the original FORTRAN version are included in the openscm-runner (Nicholls et al., 2021). Clearly the results are not very different between the two versions.
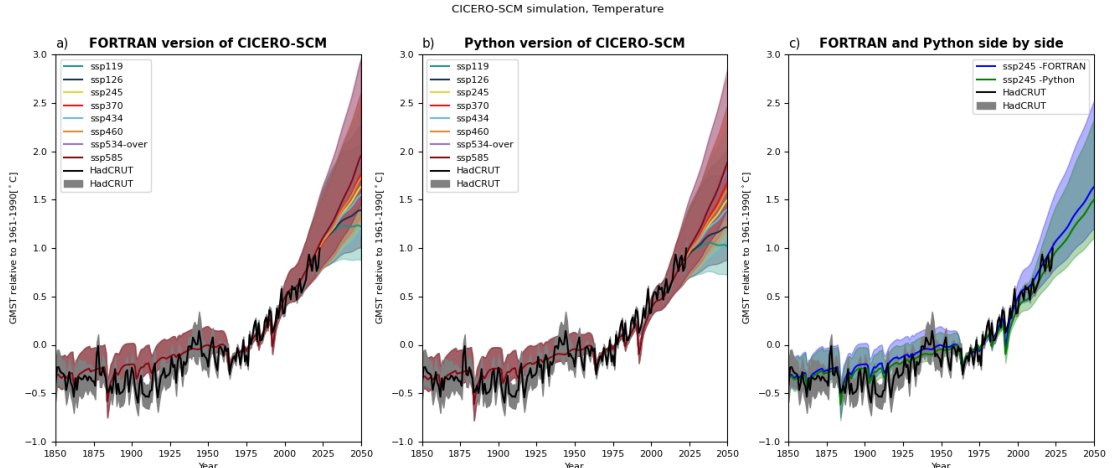
Figure 7: Shows how GMST from the ensemble used for the AR6 report (Kikstra et al., 2022; Smith et al., 2021b) as run with the current updated version, and the old FORTRAN version panel a) and in the new Python version panel b), compared to observations from the observational dataset HadCRUT (Morice et al., 2021). In panel c) for easier comparison, only the results for ssp245 are shown for both the FORTRAN version (in blue) and the Python version (in green). The comparison between the plots mainly shows that the ported Python version reproduces the old results quite faithfully given the same parameter set, though there are some changes, generally making the FORTRAN version a bit warmer than the Python version given the exact same parameters.

2.4 New parallel and calibration tools

Additions to the Python version are integrated parallelisation and calibration tools. These include the options to run over a parameter distribution set defined in a json-file or over multiple scenarios in parallel, or some combination of both.

The parameter distribution may also be generated using the calibration tools, these can both simply be used to produce either a latin hypercube or Gaussian distributions of a given size over any subset of the tunable parameters to be run over directly, or saved as a json-file for later use, or they can be used to tune parameters over such a prior distribution to fit the distribution of one or more output parameters, resulting in a tuned parameter ensemble to be run over, and saved in a json-file for later use.

The calibrator tool fits a set of n-samples to distribution functions for some subset of the parameters. The priors over the distribution space can be Gaussian or latin hypercubes and sampling is continued until a distribution of the required size is found. Samples are generated according to the prior and run in parallel chunks. Samples are then saved or rejected according to the calibration distribution over some outputs. In practice this is done by comparing its placement in the distribution for each variable to a random number, and keeping samples that are placed closer to the mean than the random number. Be aware that the larger the calibration space, i.e. the dimensionality (number of parameters) and range of the prior parameter distribution, and the higher the number of datapoints to fit to, the higher the fraction of rejection, and the higher the number of chosen samples needed to get a good fit. There is also a tunable cap on total sampling to avoid infinite looping. With non-

575 informative priors, the calibration might also need to be run for very many loops to get the required number of samples. Since quite a few of the parameters are independent, relating to specific components and diagnostics, a less compute intensive calibration workflow might be tuning only a small subset of parameters separately to various outputs at a time. For instance, carbon cycle parameters can first be tuned to reproduce CO_2 concentration timeseries, before tuning forcing and climate sensitivity or other energy balance model parameters to get observed ocean heat content and temperature change

580 distributions. Below we demonstrate how the calibration can be used to get a parameter distribution.

As a proof of concept, we've produced 100-member ensemble of parameter sets, calibrating the parameters W (vertical velocity) and lambda (the climate sensitivity parameter) from the *pamset_udm* and qindso2 (ERFaci in *ref_year*) from the *pamset_emiconc*, keeping all other parameters at default values. Parameter ranges were 0.55-6, 0.5-1.25 and -1.75- -0.25 respectively. The calibration was made to fit observed temperatures from HadCrut (Morice et al., 2021) and ocean heat

585 content from GCOS (von Schuckmann et al., 2023) timeseries including uncertainties. However, not to make the fit too difficult for a quick demonstration, only data from every 30th year of the timeseries were used. Other approaches to the exact calibration could be fitting the overall rmse between data and observations for the whole timeseries or fitting mean difference in time windows. For an even better fit more of the data should be used, more parameters might need to get fitted, and a larger ensemble should be constructed. Uncertainties that cannot be modelled with this setup, but still exist include

590 input data uncertainty. The aerosol forcing calibration in this model, can also only scale the aerosol forcing overall, and not span uncertainties in its overall time evolution. Fig. 8 shows how the 100-member calibrated set compares to the observational datasets in practice.
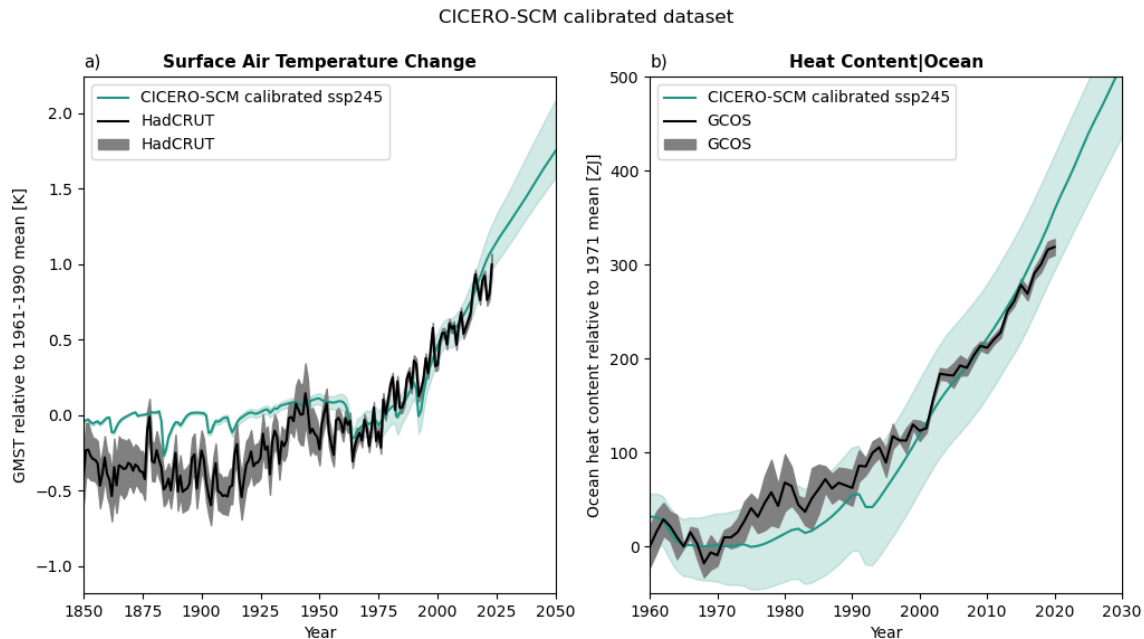
Figure 8: Results from a 100 member ensemble calibrating qindso2, W and lambda to fit observed temperature from HadCrut (Morice et al., 2021) and total ocean heat content from GCOS (von Schuckmann et al., 2023). Part a) shows the temperature for the 2.5th to the 97.5th percentile compared to the same in the HadCRUT dataset, part b) shows the ocean heat content 5th to 90th percentile compared to the same in GCOS. GMST (Surface Air Temperature Change) is shown as change relative to 1961-1990 period, while ocean heat content is shown relative to 1971 ensemble mean values.

3 Conclusions

In this paper we have described the CICERO-SCM simple climate model in its current incarnation as a Python implemented open-source model. Though the model has been improved in terms of readability and user friendliness, opportunities for further development abound. There are also many questions that the model is not currently suited to answer, that it could be adapted towards answering.

In terms of technical modifications, the Python version is still slower than the FORTRAN model, and opportunities for further speed-ups should be explored. Quite some time could likely be shaved off the run-time using more efficient data structures and calculations. However, such modifications may also come at the expense of readability or easy model adaptation to new usages. Making the calibration more efficient, flexible, and statistically robust is also a technical priority. Eventually producing and updating calibrated parameter sets that represent good fits to current available knowledge being the end goal of such an exercise. Keeping the model up to date with libraries and packages should also be a part of the development moving forward.

As for the functionality, the current modular structure allows for parts of the model to be used independently and provides options to change either the emissions to forcing or energy balance model with different models altogether. This could allow for testing and updating, for instance using a more efficient ocean model with fewer layers, or having a simpler, faster, and less readable emissions to forcing module, which can be interchanged with the current more readable, adaptable, yet slower version. Though we acknowledge that modularity could be improved further – for example, isolating the carbon cycle module.

Some updates that could open up for explorations of questions the model currently doesn't answer properly include, but is not limited to; regionalization of the temperature response, inclusion of temperature feedbacks into the carbon uptake, component breakdown of the carbon cycle keeping track of the carbon amounts in the various pools (representing processes which impact both heat and carbon transport in the ocean, for example), a more proper treatment of aerosol cloud interactions to account for time delays in cloud formation (Jia and Quaas, 2023), inclusion of nitrate aerosols, updated formulas for O_3 ERF and updated CH_4 lifetime treatments reproducing more recent atmospheric chemistry model results (Skeie et al., 2023; Stevenson et al., 2020), continuous updates of lifetimes and forcing strength for various compounds, inclusion of more compounds thought to have a climate impact in the future, such as for instance molecular hydrogen

(Hauglustaine et al., 2022; Paulot et al., 2021; Sand et al., 2023; Warwick et al., 2023) or ammonia (NH_3) (Bertagni et al., 2023).

630 In general, we hope that this open, accessible version of the model will facilitate expanded use, and community development of the model and hope to see colleagues and users engage with it in whatever way they find most useful.

4 Appendices

4.1 Appendix A – Default plots from a run with all parameters set to default values

The module includes automatic plotting options. Using these options, we can plot the time evolution of emissions, 635 concentrations and forcing changes per component. As well as ocean heat content change, radiative imbalance and temperature change. Below, such plots from a run with all parameter values set to default values run with the historical CMIP6 input data are shown:
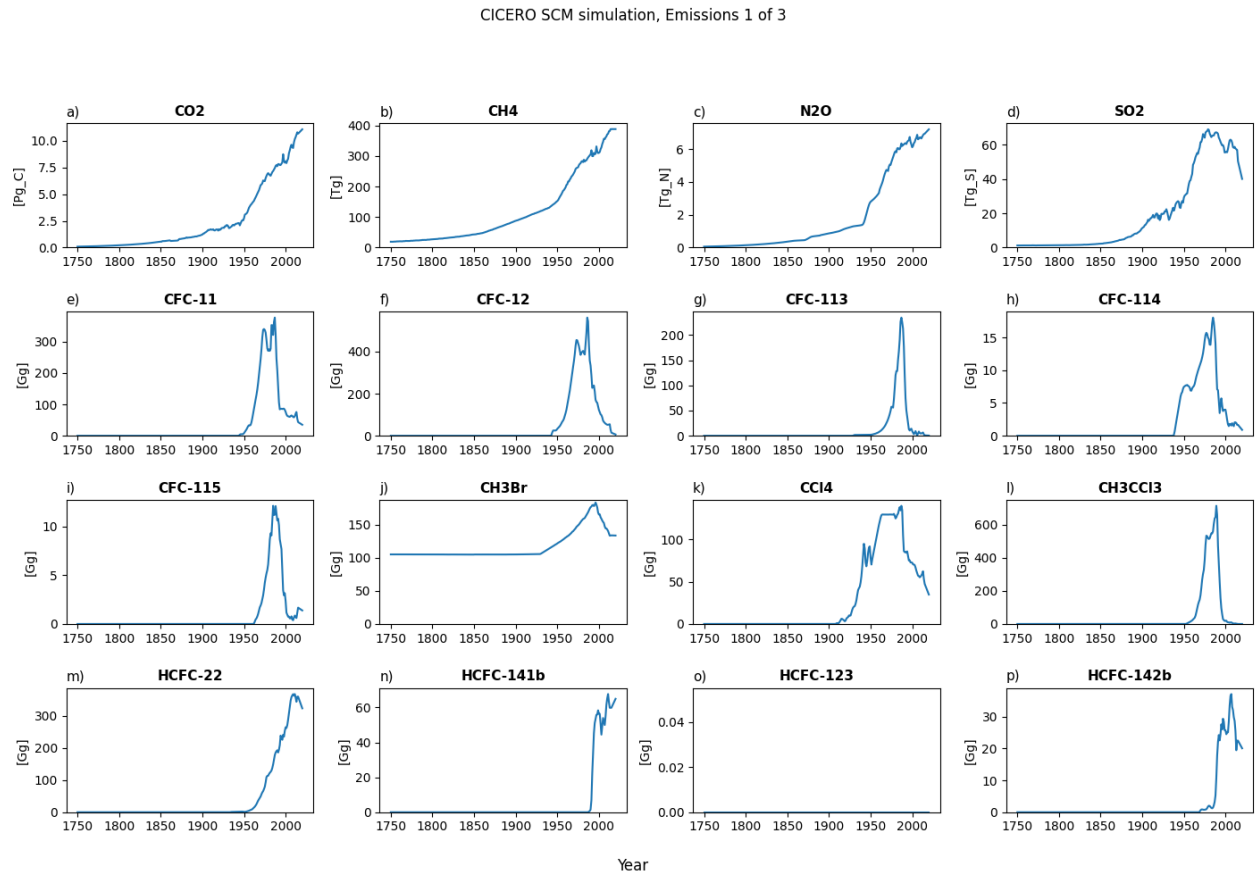
Figure A1: Default emissions output plot number 1 for a run with default parameters using historical emissions up to 2014 and

 ssp245 emission year 2014 to the end year 2020 all from RCMIP (Nicholls et al., 2020). The input dataset did not include data for HCFC-123, hence the values for this gas is zero throughout.
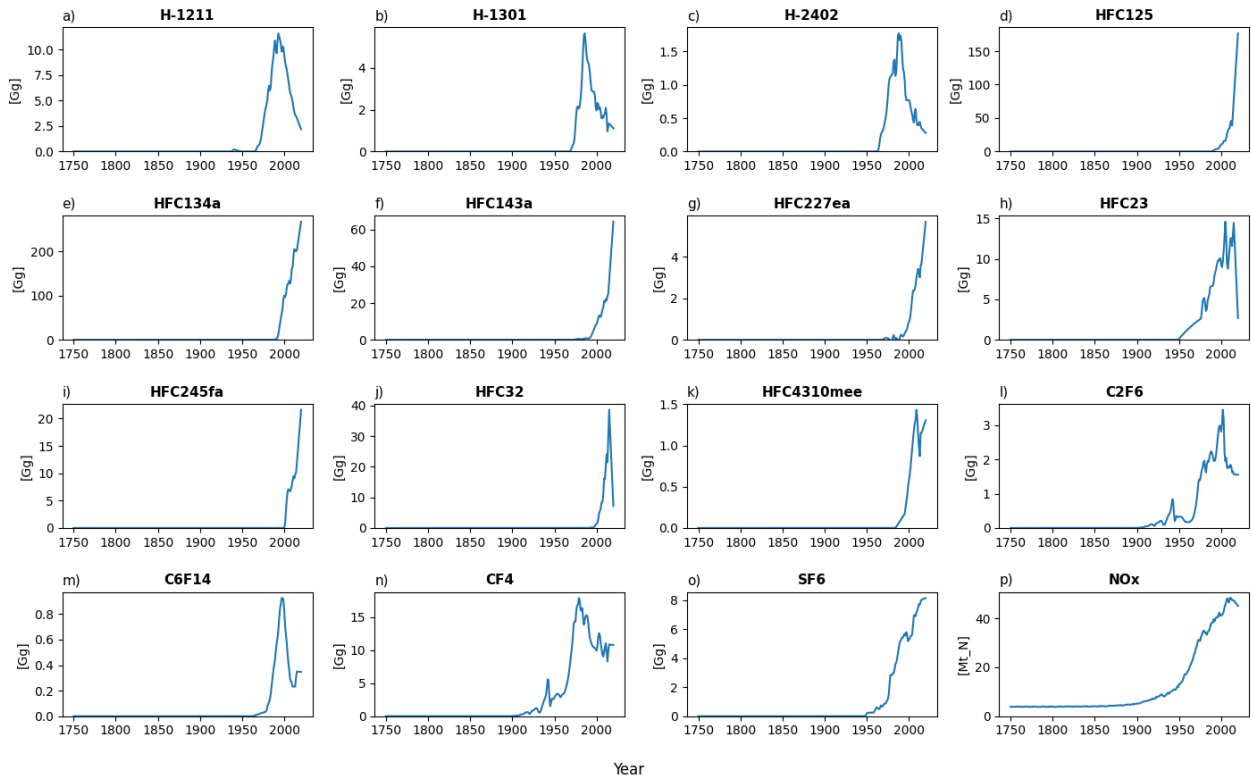
Figure A2: Default emissions output plot number 2 for a run with default parameters of the historical emissions up to 2014 and
645   **ssp245 emission year 2014 to the end year 2020 all from RCMIP (Nicholls et al., 2020).**
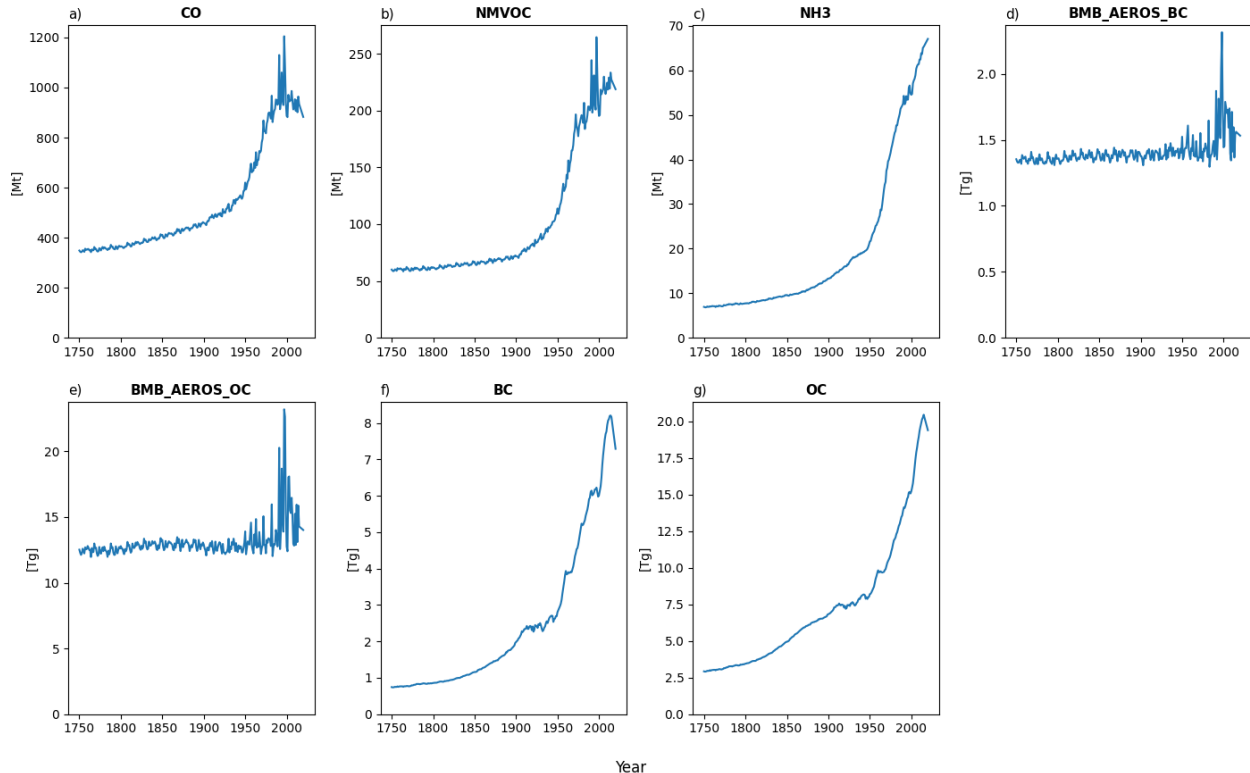
Figure A3: Default emissions output plot number 3 for a run with default parameters of the historical emissions up to 2014 and ssp245 emission year 2014 to the end year 2020 all from RCMIP (Nicholls et al., 2020).
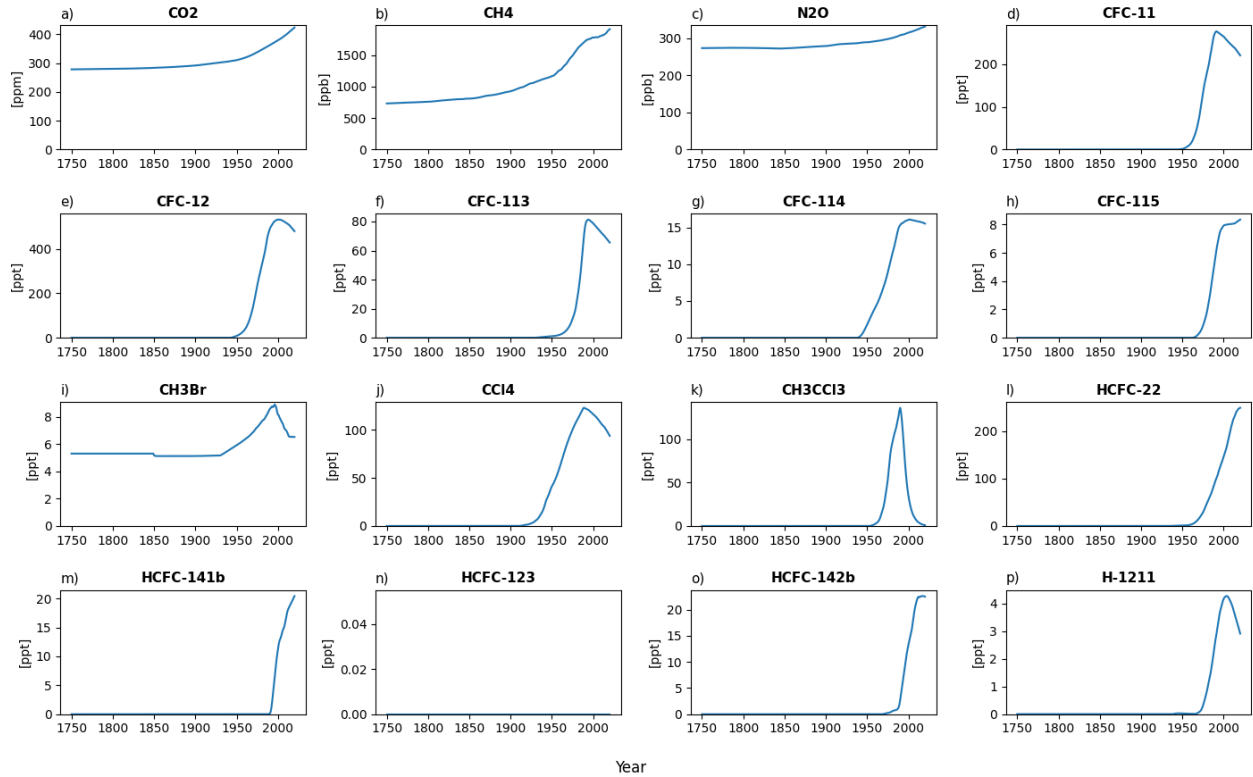
650

Figure A4: Default concentration output plot number 1 for a run with default parameters of the historical emissions up to 2014 and ssp245 emission year 2014 to the end year 2020 all from RCMIP (Nicholls et al., 2020). The input dataset did not include data for HCFC-123, hence the values for this gas is zero throughout.
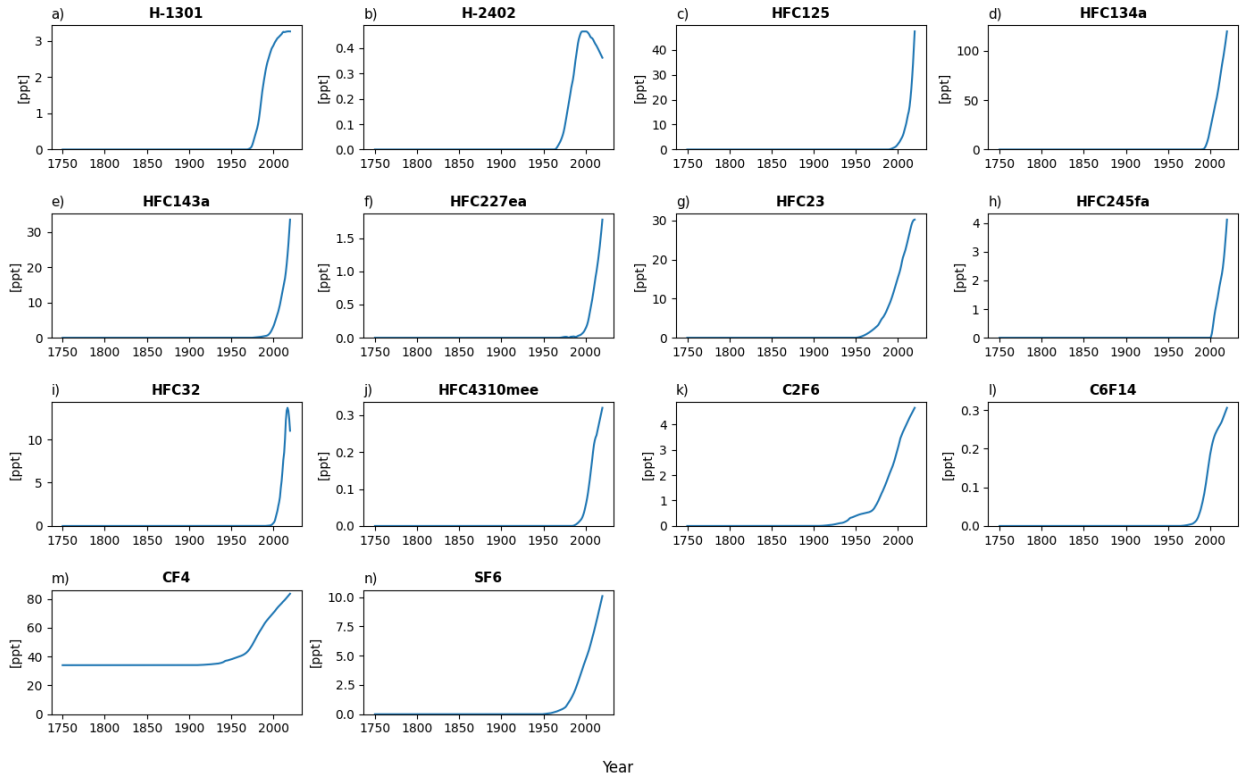
655

Figure A5: Default concentration output plot number 2 for a run with default parameters of the historical emissions up to 2014 and ssp245 emission year 2014 to the end year 2020 all from RCMIP (Nicholls et al., 2020).
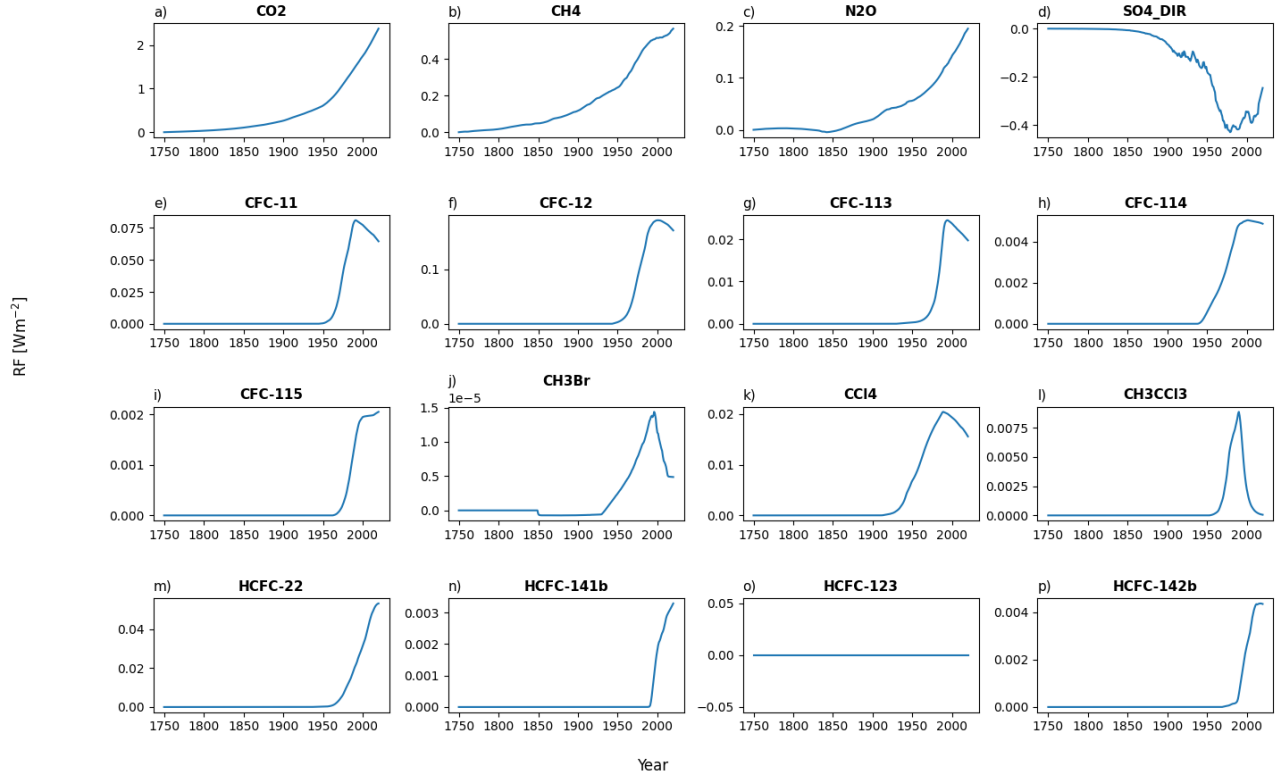
660

Figure A6: Default forcing output plot number 1 for a run with default parameters of the historical emissions up to 2014 and ssp245 emission year 2014 to the end year 2020 all from RCMIP (Nicholls et al., 2020). The input dataset did not include data for HCFC-123, hence the values for this gas is zero throughout.
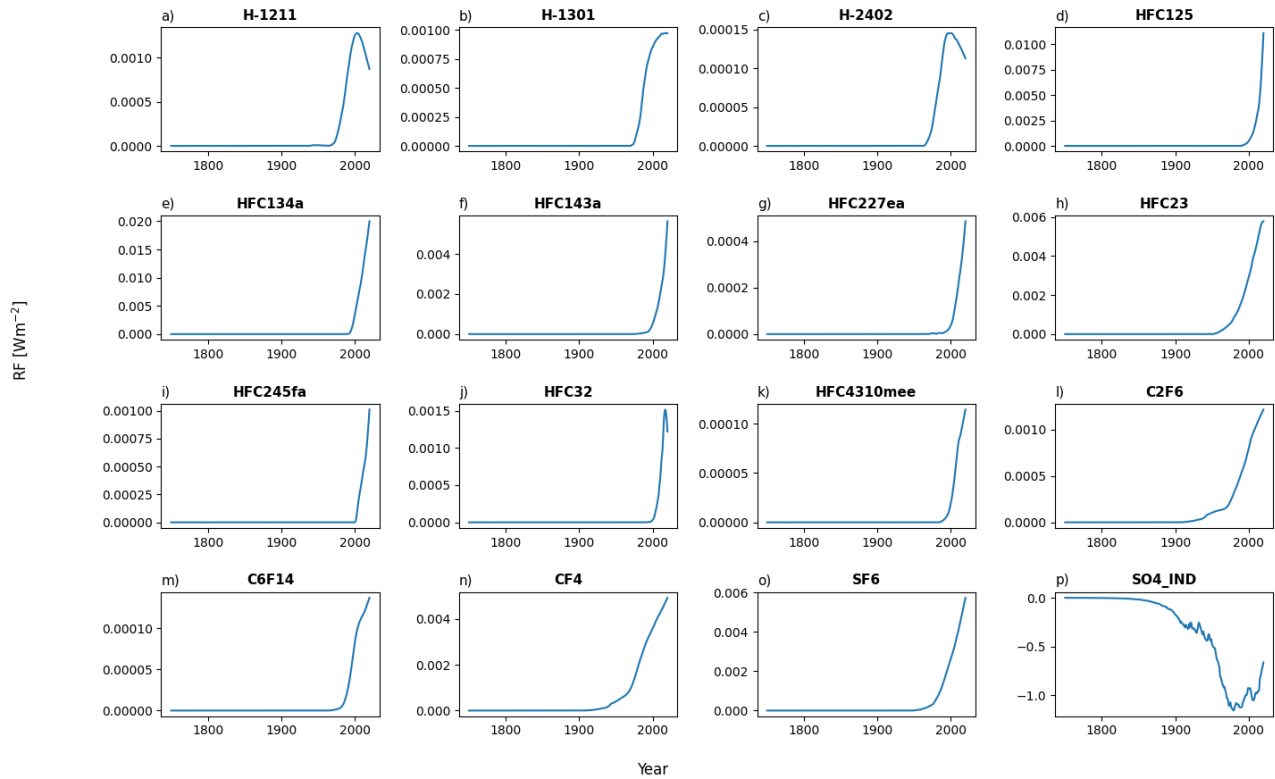
665 **Figure A7: Default forcing output plot number 2 for a run with default parameters of the historical experiment emissions up to 2014 and ssp245 emission year 2014 to the end year 2020 all from RCMIP (Nicholls et al., 2020).**
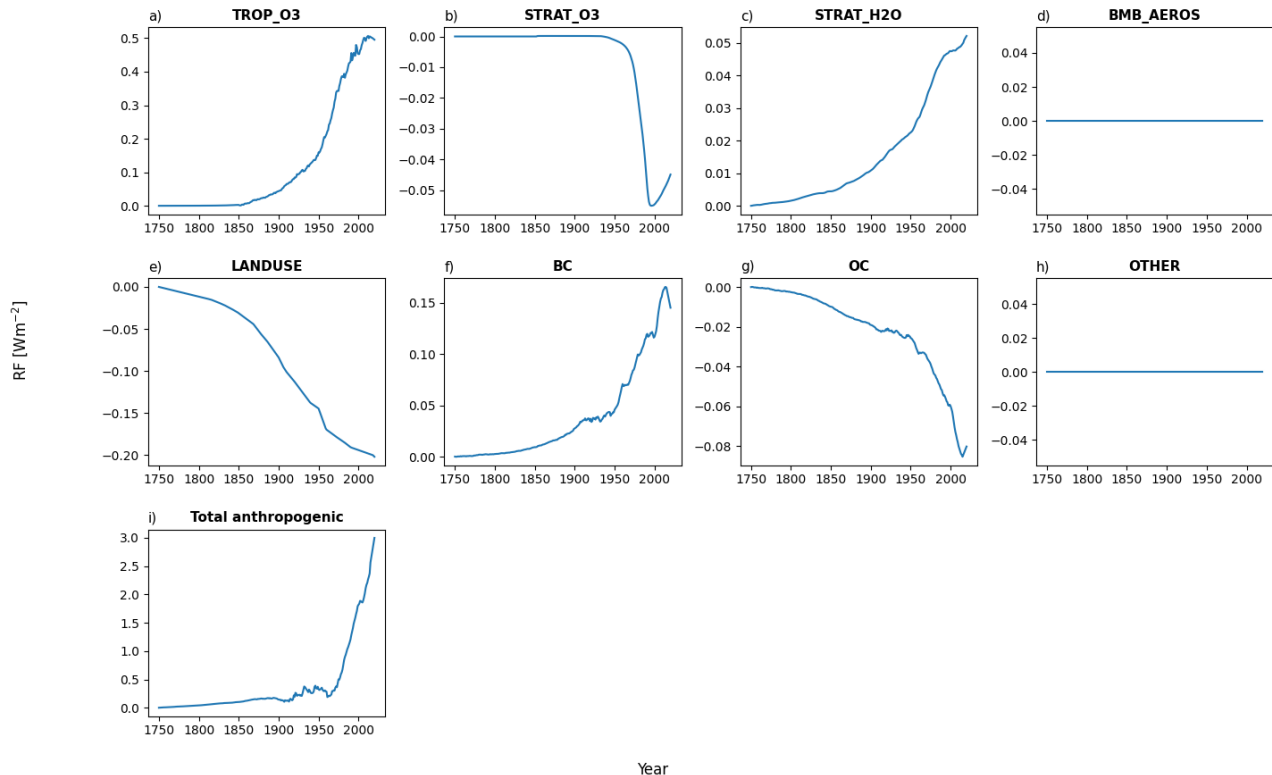
Figure A8: Default forcing output plot number 3 for a run with default parameters of the historical emissions up to 2014 and ssp245 emission year 2014 to the end year 2020 all from RCMIP (Nicholls et al., 2020). The default settings for the model has qbmb the forcing scaling for biomass burning aerosols set to zero, hence the BMB_AEROS forcing timeseries is zero throughout

670
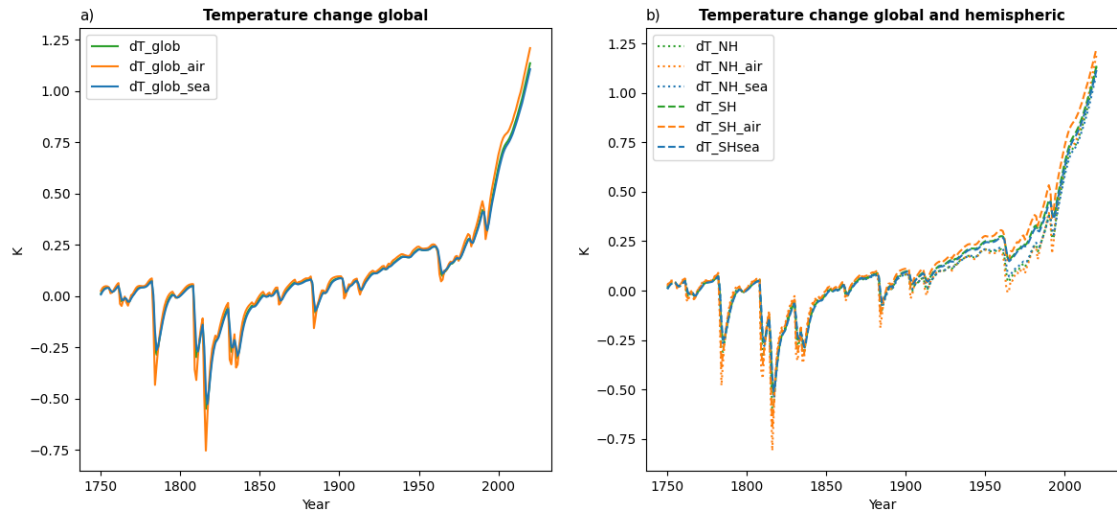
Figure A9: Default temperature change since 1750 output plot for a run with default parameters of the historical emissions up to 2014 and ssp245 emission year 2014 to the end year 2020 all from RCMIP (Nicholls et al., 2020).

675
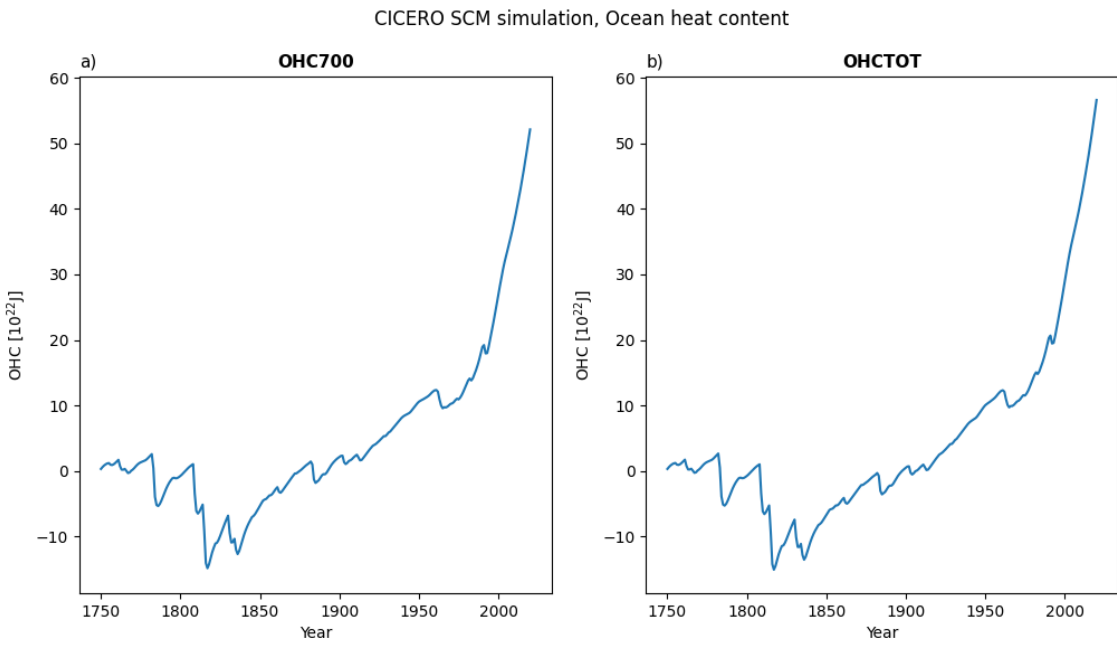
Figure A10: Default output plot of ocean heat content change since 1750 for a run with default parameters of the historical emissions up to 2014 and ssp245 emission year 2014 to the end year 2020 all from RCMIP (Nicholls et al., 2020).
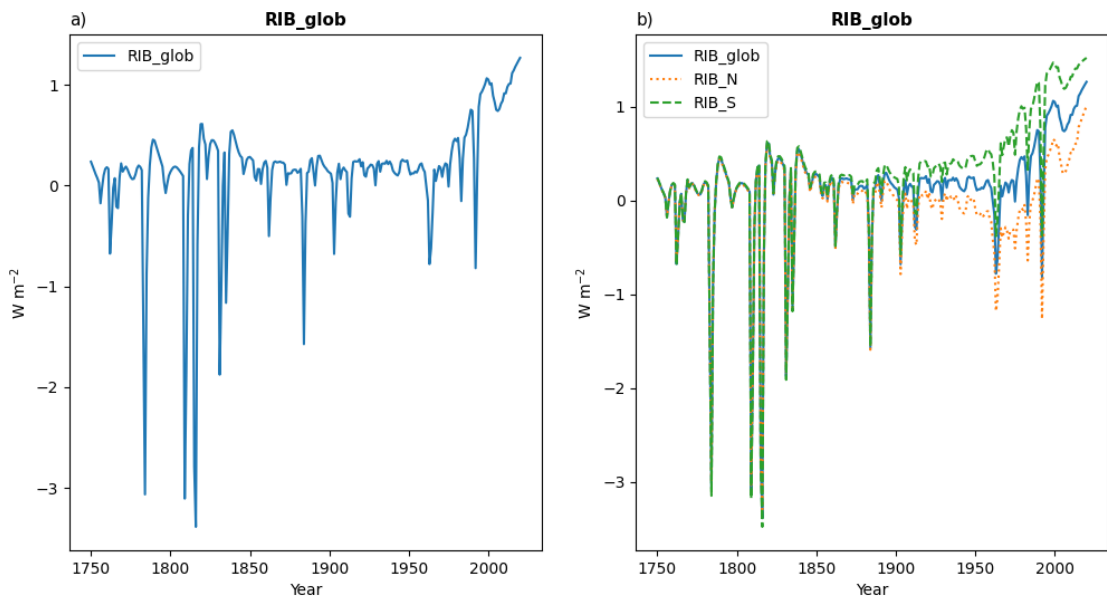
Figure A11: Default plot of radiative imbalance change since 1750 for a run with default parameters of the historical emissions up to 2014 and ssp245 emission year 2014 to the end year 2020 all from RCMIP (Nicholls et al., 2020).

4.2 Appendix B - Natural emissions estimates for CH₄ and N₂O

CH$_4$ and N$_2$O both have considerable natural emissions contributions (Saunois et al., 2020; Tian et al., 2020). In the model timeseries of these can be fed as separate files or dataset timeseries to the model instance. If not sent, a flat natural emissions value from the gaspam-file will be sent. However, using a flat natural emissions timeseries will rarely give a good match to observed concentrations, so the model also comes with a preprocessing script to generate natural emissions time series. Using a precalculated time series from a different model setup, or input dataset, will lead to different fits to concentration time series for both components. But a finely tuned input time series, will also make the emissions to concentration calculation for these species superfluous, as the natural emissions are constructed to fit whatever is missing from the anthropogenic distribution, and the run will effectively be concentration driven for these components.

In the FORTRAN version the method for calculating the natural emissions time series used a calibration per time step method, iterating and adjusting the natural emissions from the previous step by five percent until the concentration matched with less than five percent discrepancy. As we know that we have an exact solution for converting emissions to concentrations in each timestep, though, we can solve the equation exactly for the missing emissions in each time step for a much more efficient, though somewhat more noisy solution. Both options are available as options from the *precalculate_natural_emissions.py* script in the scripts/prescripts subfolder. When the historical data finishes, the future value of natural emissions is however assumed constant with a value that is the mean of the last 11 values. Figure A1 shows

these estimates from CMIP6 (Smith et al., 2021b) concentration data as used throughout this article, alongside the input anthropogenic emissions and the flat emissions from the default gaspam_file.
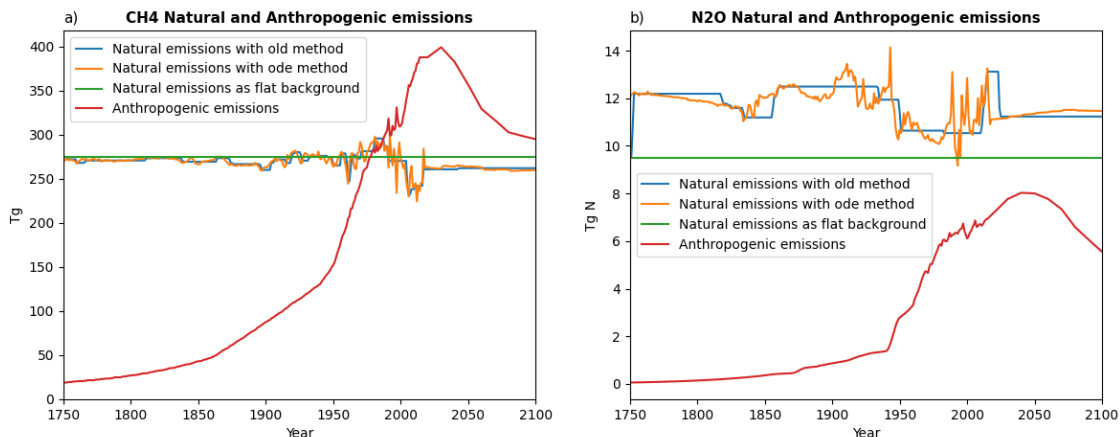
Figure B1: Timeseries of the estimated natural emissions and anthropogenic input emissions for historical and the ssp245 scenario for CH₄ and N₂O. The old data is data constructed using the method used to make natural emissions for the FORTRAN model. The ode method is using script that is included with the Python version relying on the exact solution. In both cases the "TAR" lifetime mode for CH₄ is used for the estimates. The flat background is the flat natural emissions value from the gaspam_file (Table 3).

For CH₄, the amount of estimated natural emissions will vary significantly with choice of lifetime mode, as the natural emissions are effectively masking over whatever is needed to make up the expected concentration time series. For now, this means that running the model with estimated natural emissions, we are effectively only modelling CH₄ and N₂O forcing from concentrations in the historical period. The choice of lifetime mode may play a much larger part, when natural emissions are unknown and estimated using a flat background value, or a flat mean as the script calculates for the future.

Figure A2 shows how the lifetime of CH₄ evolves using different lifetime modes. It also displays how different the natural emissions estimates are depending on which lifetime mode is chosen.

715

4.3 Appendix C - Upwelling diffusion model equations

The equations used to describe the how energy is exchanged through the ocean system can be found in appendix B of (Schlesinger et al., 1992). They consist of differential equation sets for each of the layers in the ocean, accounting for all processes transporting heat in and out of the layer in each hemisphere. The equation for each hemisphere is completely

720 symmetrical, so we will state only the equations for the Northern Hemisphere here for simplicity. The equations include terms relating to heat transfer between the hemispheres, and these terms are even included in the code and scaled by the atmospheric interhemispheric heat exchange parameter β_a (ebbeta). However, we will omit these terms here, as the equations simplify without them, and the parameter is mostly not used.

In the mixed (uppermost) ocean layer, the equation reads:

725
$$\gamma_N \, \rho c \Delta z_1 \frac{\delta T_1}{\delta t} = q - \lambda T_1 + 2\gamma_N \rho c_p \kappa \frac{T_2 - T_1}{\Delta z_2} + \gamma_N \rho c_p W (T_1 - T_P) - \gamma_N \beta_o (T_1 - T_{1,S}) \qquad (S1)$$

where $\gamma_N = \sigma_N + \frac{\lambda}{\lambda_{a,o}}$, with σ_N the Northern Hemisphere ocean fraction (foan), and $\lambda_{a,o}$ (rlamdo) the air-sea heat exchange parameter and λ the equilibrium climate sensitivity divided by 2xCO2 radiative forcing (see Table 4 for details and units). Both temperature and forcing values all denote changes from the temperature and forcing at the start of the model run, rather than absolute temperatures. Subscript numbers denote the ocean layer number, counted from the top, so layer 1 is the

730 mixed layer. All quantities are the versions of the quantities in the Northern hemisphere non-polar ocean unless otherwise specified. $T_{1,S}$ is the temperature in the Southern Hemisphere, T_P is the Northern Hemisphere polar ocean temperature assumed to change according to B8 of (Schlesinger et al., 1992), i.e. just following the change in the main ocean temperature mixed layer times Π (the cpi parameter in Table 4).

$$T_p = \Pi \cdot T_1 \qquad (S2)$$

735

q is the Northern Hemisphere forcing (in Wm^{-2}), ρ is the seawater density (1030 kg m^3), c_p is the specific heat capacity of seawater ($3.997 \cdot 10^3 \frac{J}{kg\,K}$), Δz_l is the height of layer l in meters . κ is the vertical heat diffusivity (akapa), β_o is the oceanic interhemispheric heat exchange rate (beto) and W is the upwelling rate. These three are tunable parameters (see Table 4 for details and units). Finally, when the parameter threstemp is non-zero, the upwelling rate

740 W, is not equal to the parameter W in Table 4, but it is rather given as:

$$W = W_{\text{Table 4}} \cdot \left(1 - \frac{10}{3} \cdot \frac{T_1}{T_{\text{thres}}}\right) \qquad (S3)$$

i.e. the threstemp parameter is the mixed layer temperature change at which the upwelling velocity decreases by 30%. This decrease in upwelling velocity was not included in the model described in (Schlesinger et al., 1992), but is an updated based on the work of (Raper et al., 2001).

745 To simplify the equations, atmospheric transport between the hemispheres is assumed to be zero in this derivation, though it is included in the code and its strength is controlled by the parameter ebbeta (β_a).

The left-hand side represents the rate of change of energy in the mixed layer, where the γ_N factor accounts for heat exchange between the ocean and the atmosphere (and when β_a is included also with atmospheric interhemispheric heat exchange). Examining the terms on the right-hand side, they represent radiative forcing, then the temperature longwave radiation and

750 climate feedback, then the vertical diffusion heat transport to the layer below, then vertical advective heat transport into the polar ocean and finally interhemispheric heat transport. The polar ocean temperature is assumed to be ΠT_1 throughout.

For all internal ocean layers the equation is:

$$\rho c_p \Delta z_k \frac{\delta T_k}{\delta t} = \rho c_p \left[2\kappa \frac{T_{k+1} - T_k}{(\Delta z_k + \Delta z_{k+1})} + W \cdot T_{k+1} \right] - \rho c_p \left[2\kappa \frac{T_k - T_{k-1}}{(\delta \Delta z_k + \Delta z_{k-1})} + W \cdot (\delta T_k + (1 - \delta) T_{k-1}) \right] - \beta_o (T_k - T_{k,S}) \tag{S4}$$

Here, we have the rate of change of energy per area in the layer on the left, diffusion and advection with the layer below first,

755 then diffusion and advection with the layer above, and finally interhemispheric heat transport across the horizontal boundary. The δ in the denominator of the diffusion term and in the second advection term is 0 for the uppermost of the layers, and 1 otherwise. In the equation for the Southern hemisphere, this last term will also be scaled by the ratio between the two ocean surfaces to ensure an equal amount of heat is accounted for as seen from both hemispheres. Note also that in the original formulation in (Schlesinger et al., 1992), the advection terms did not depend on the temperature in the layer from which the

760 advection came, i.e. they were not on the form given here of $\rho c_p \cdot W \cdot T_{k+1}$ and $\rho c_p \cdot W \cdot T_k$, but rather on the average temperature between the layer from which the advection came and the one it advected into, i.e. on the form $\rho c_p \cdot W \frac{T_{k+1} + T_k}{2}$ and $\rho c_p \cdot W \frac{T_{k-1} + T_k}{2}$. The same was true for the advection out of the bottom layer (see equation S5).

For the ocean bottom layer L, the equation reads:

$$\rho c_p \Delta z_L \frac{\delta T_L}{\delta t} = -\rho c_p \left[2\kappa \frac{T_L - T_{L-1}}{(\Delta z_L + \Delta z_{L-1})} + W \cdot T_L \right] + \rho c_p W T_P - \beta_o (T_L - T_{L,S}) \tag{S5}$$

765 Where there is no longer any heat transported from the layer below, as there is none, however, we also account for transport of heat from the bottom of the polar ocean, and transport to the Southern Ocean. In other words, in the model heat is transferred into the polar ocean at the top and transported back in from it at the bottom layer.

Now, for the solution of this equation set in the code, the solution involves a separation of terms. First for the forcing, interhemispheric heat-exchange terms and polar heat exchange terms, a simple forward Euler solution, $\delta T_k(t) \approx T_k(t) -$

770 $T_k(t - 1)$ is employed in gathering all these terms in one and solving for them in all layers first. These are then added to the equations and can be viewed as constant terms in the further differentiation. Then the climate feedback, diffusion and

advection terms are combined in a backward implicit Euler calculation. I.e., the equations are solved assuming all these terms are given for the current timestep, and we solve the equations for them.

We rewrite the top layer eq. (S1) as

$$\gamma_N \, \rho c_p \Delta z_1 \frac{\delta T_1}{\delta t} = q - \lambda T_1 + 2\gamma_N \rho c_p \kappa \frac{T_2 - T_1}{\Delta z_2} + \gamma_N \rho c_p W (T_1 - T_P) - \gamma_N \beta_o (T_1 - T_{1,S}) \tag{S1}$$

$$\gamma_N \, \rho c_p \Delta z_1 \frac{T_1(t) - T_1(t-1)}{dt} - 2\gamma_N \rho c_p \kappa \frac{T_2 - T_1}{\Delta z_2} - \gamma_N \rho c_p W T_1 = q - \lambda T_1 - \gamma_N \rho c_p W \Pi T_1 - \gamma_N \beta_o (T_1 - T_{1,S}) \tag{S6}$$

Unless otherwise stated, LHS is time t, RHS is time t-1 Dividing by $\frac{\gamma_N \, \rho c_p \Delta z_1}{dt}$:

$$T_1(t) - T_1(t-1) - \frac{2\kappa dt}{\Delta z_1 \Delta z_2}(T_2 - T_1) - \frac{W dt}{\Delta z_1} T_1 = \frac{q dt}{\gamma_N \, \rho c_p \Delta z_1} - \frac{\lambda dt}{\gamma_N \, \rho c_p \Delta z_1} T_1 - \frac{W \Pi dt}{\Delta z_1} T_1 - \frac{\beta_o dt}{\rho c_p \Delta z_1}(T_1 - T_{1,S}) \tag{S7}$$

$$\left(1 + \frac{\lambda dt}{\gamma_N \, \rho c_p \Delta z_1} + \frac{2\kappa dt}{\Delta z_1 \Delta z_2} - \frac{W dt}{\Delta z_1}\right) T_1 - \frac{2\kappa dt}{\Delta z_1 \Delta z_2} T_2 = \left(1 - \frac{W \Pi dt}{\Delta z_1} - \frac{\beta_o dt}{\rho c_p \Delta z_1}\right) T_1 + \frac{\beta_o dt}{\rho c_p \Delta z_1} T_{1,S} + \frac{q dt}{\gamma_N \, \rho c_p \Delta z_1} \tag{S8}$$

Note, for shorthand, LHS is time t, RHS is time t-1

The equation set can in principle can be written this way for the various layers:

$$b_1 T_1 + c_1 T_2 = d_1, \qquad a_k T_{k-1} + b_k T_k + c_k T_{k+1} = d_k, \qquad a_L T_{L-1} + b_L T_L = d_L \tag{S9}$$

In the code we go through the equations and find the coefficients a_k, b_k and c_k. The d_k terms are the results of the forward Euler solution for the horizontal transport. This now defines a banded matrix problem and can be solved using a suitable banded matrix solver.

Following this approach, the coefficients a_1, b_1, and d_1 are:

$$b_1 = 1 + \frac{\lambda dt}{\gamma_N \, \rho c \Delta z_1} + \frac{2\kappa \, dt}{\Delta z_1 \Delta z_2} - \frac{W \, dt}{\Delta z_1}, \quad c_1 = -\frac{2\kappa \, dt}{\Delta z_1 \Delta z_2},$$

$$d_1 = \left(1 - \frac{\Pi W dt}{\Delta z_1} - \frac{\beta_o dt}{\rho c_p \Delta z_1}\right) T_1(t-1) + \frac{\beta_o dt}{\rho c_p \Delta z_1} T_{1,S}(t-1) + \frac{q \, dt}{\gamma_N \rho c_p \Delta z_1} \tag{S10}$$

where q is now the mean forcing over the preceding year.

Performing similar transformations as for the top layer on eq. (S4), the coefficients for the internal layers a_k, b_k, c_k and d_k become:

$$a_k = -\frac{2\kappa \, dt}{\Delta z_k (\delta \Delta z_k + \Delta z_{k-1})} + (1 - \delta)\frac{W \, dt}{\Delta z_k}, \qquad b_k = 1 + \frac{2\kappa \, dt}{\Delta z_k (\Delta z_{k-1} + \delta \Delta z_k)} + \frac{2\kappa \, dt}{\Delta z_k (\Delta z_{k+1} + \Delta z_k)} + \delta \frac{W \, dt}{\Delta z_k},$$

$$c_k = -\frac{2\kappa \, dt}{\Delta z_k (\Delta z_{k+1} + \Delta z_k)} - \frac{W \, dt}{2\Delta z_k},$$

$$d_k = \left(1 - \frac{\beta_o dt}{\rho c_p \Delta z_k}\right) T_k(t-1) + \frac{\beta_o dt}{\rho c_p \Delta z_k} T_{k,S}(t-1), \tag{S11}$$

where δ in the expressions for a_k and b_k is 0 for the second layer and 1 otherwise.

And for the bottom layer (from eq. (S5)):

$$a_L = -\frac{2\kappa\, dt}{\Delta z_L(\Delta z_L + \Delta z_{L-1})}, \qquad b_L = 1 + \frac{2\kappa\, dt}{\Delta z_L(\Delta z_L + \Delta z_{L-1})} + \frac{W\, dt}{\Delta z_L}, \qquad c_L = 0,$$

$$d_L = \left(1 - \frac{\beta_o dt}{\rho c_p \Delta z_L}\right) T_L(t-1) + \frac{\beta_o dt}{\rho c_p \Delta z_L} T_{L,S}(t-1) + \frac{\Pi W dt}{\Delta z_L} T_1(t-1) \qquad (S12)$$

5 Code availability

The Python code is openly available on github at https://github.com/ciceroOslo/ciceroscm with a zenodo doi for the version used here https://doi.org/10.5281/zenodo.10548720.

The FORTRAN version of the code is not open as such, but executable versions for various operating systems are available as part of the openscm-runner framework https://github.com/openscm/openscm-runner (last accessed 16.01.2024).

6 Data availability

RCMIP (Nicholls et al., 2020) input data used for running the models and most plots are available from here https://gitlab.com/rcmip/rcmip with a zenodo doi (Nicholls and Gieseke, 2019).

Model output has also been compared with forcing and temperature output from IPCC AR6 chapter 7 (Smith et al., 2021a), with HadCrut temperature data (Morice et al., 2021), and GCOS ocean heat content data (von Schuckmann et al., 2023), all openly available datasets.

7 Author contributions

MS was the main developer for the porting of the code to python, and also the main author of the paper. BA contributed with comments to improve the manuscript and code from a user perspective. ANJ contributed to the codes additional features and proof-read the manuscript. MTL and RBS helped ensure a faithful rendition of the features of the Fortran original and various related tools and contributed heavily to the scientific choices made in the code improvements, plots, and text, and made initial drafts. GPP laid the groundwork for the text in the introduction, and several other sections, and contributed heavily to a clearer understanding of the natural emissions approach in Appendix A and of the upwelling diffusion model in Appendix B. BMS contributed to the coding process and in doing code reviews and wrote the sections on the carbon cycle. BHS, GPP, and RBS provided the momentum to get the process for the porting project started and obtained the funding necessary to do it from various sources. All authors have read the paper and contributed comments and improvements.

8 Competing interests

The authors declare that they have no conflict of interest.

9 Acknowledgements

We acknowledge CICERO, for yearlong support and funding for this model and its maintenance and development in terms of both human and computational resources. The Norwegian research council project UTRICS (grant no. 314997) has contributed funding for the process of writing this article and adding calibration and parallelisation tools. European Union Horizon 2020 project PROVIDE (grant agreement No. 101003687) has also provided funding for testing and improvements and for the work of BMS.

10 References

Aamaas, B., Peters, G. P., and Fuglestvedt, J. S.: Simple emission metrics for climate impacts, Earth Syst. Dynam., 4, 145–170, https://doi.org/10.5194/esd-4-145-2013, 2013.

Aldrin, M., Holden, M., Guttorp, P., Skeie, R. B., Myhre, G., and Berntsen, T. K.: Bayesian estimation of climate sensitivity based on a simple climate model fitted to observations of hemispheric temperatures and global ocean heat content, Environmetrics, 23, 253–271, https://doi.org/10.1002/env.2140, 2012.

Alfsen, K. H. and Berntsen, T. K.: An efficient and accurate carbon cycle model for use in simple climate models, CICERO Center for International Climate and Environmental Research - Oslo, 1999.

Atjay, G. L., Ketner, P., and Duvigneaud, P.: Terrestrial primary production and phytomass, in: The Global Carbon Cycle [Bolin, B., E.T. Degens, S. Kempe, and P. Ketner (eds.), Wiley & Sons, Chichester, 129–181, 1979.

Balaji, V., Maisonnave, E., Zadeh, N., Lawrence, B. N., Biercamp, J., Fladrich, U., Aloisio, G., Benson, R., Caubel, A., Durachta, J., Foujols, M.-A., Lister, G., Mocavero, S., Underwood, S., and Wright, G.: CPMIP: measurements of real computational performance of Earth system models in CMIP6, Geoscientific Model Development, 10, 19–34, https://doi.org/10.5194/gmd-10-19-2017, 2017.

Bertagni, M. B., Socolow, R. H., Martirez, J. M. P., Carter, E. A., Greig, C., Ju, Y., Lieuwen, T., Mueller, M. E., Sundaresan, S., Wang, R., Zondlo, M. A., and Porporato, A.: Minimizing the impacts of the ammonia economy on the nitrogen cycle and climate, Proceedings of the National Academy of Sciences, 120, e2311728120, https://doi.org/10.1073/pnas.2311728120, 2023.

Boucher, O., Borella, A., Gasser, T., and Hauglustaine, D.: On the contribution of global aviation to the CO2 radiative forcing of climate, Atmospheric Environment, 267, 118762, https://doi.org/10.1016/j.atmosenv.2021.118762, 2021.

Ehhalt, DieterH., Prather, M. J., Detener, F., Derwent, R. G., Dlugokencky, E., Holland, E., Isaksen, I. S. A., Katima, J., Kirchhoff, V., and Matson, P.: Atmospheric Chemistry and Greenhouse Gases, in: Climate Change 2001: The Scientific Basis, Houghton, J.T., Ding, Y., Griggs, D.J:, Noguer, M., van der Linden, P.J., Dai, X., Maskell, K., Johnson, C.A., Cambridge University Press, United Kingdom and New York, NY USA, 2001.

den Elzen, M., Fuglestvedt, J., Höhne, N., Trudinger, C., Lowe, J., Matthews, B., Romstad, B., de Campos, C. P., and Andronova, N.: Analysing countries' contribution to climate change: scientific and policy-related choices, Environmental Science & Policy, 8, 614–636, https://doi.org/10.1016/j.envsci.2005.06.007, 2005.

855   den Elzen, M. G. J., Olivier, J. G. J., Höhne, N., and Janssens-Maenhout, G.: Countries' contributions to climate change: effect of accounting for all greenhouse gases, recent trends, basic needs and technological progress, Climatic Change, 121, 397–412, https://doi.org/10.1007/s10584-013-0865-6, 2013.

Etminan, M., Myhre, G., Highwood, E. J., and Shine, K. P.: Radiative forcing of carbon dioxide, methane, and nitrous oxide: A significant revision of the methane radiative forcing, Geophysical Research Letters, 43, 12,614-12,623, 860   https://doi.org/10.1002/2016GL071930, 2016.

Forster, P. M. de F., Ramaswarmy, V., Artaxo, P., Berntsen, T. K., Betts, R., Haywood, J., Lean, J., Lowe, D. C., Myhre, G., Nganga, J., Prinn, R. G., Raga, G., Schulz, M., and Van Dorland, R.: Changes in Atmospheric Constituents and in Radiative Forcing., in: Climate Change 2007: The Physical Science Basis. Contribution of Working Group I to the Fourth Assessment Report of the Intergovernmental Panel on Climate Change [Solomon, S., D. Qin, M. Manning, Z. Chen, M. Marquis, K.B. 865   Averyt, M.Tignor and H.L. Miller (eds.)], Cambridge University Press, Cambridge, United Kingdom and New York, NY, USA, 129–234, 2007.

Forster, P. M. de F., Storelvmo, T., Armour, K., Collins, W. J., Dufresne, J.-L., Frame, D. J., Lunt, D. J., Mauritsen, T., Palmer, M. D., Watanabe, M., Wild, M., and Zhang, H.: The Earth's Energy Budget, Climate Feedbacks, and Climate Sensitivity., in: In Climate Change 2021: The Physical Science Basis. Contribution of Working Group I to the Sixth 870   Assessment Report of the Intergovernmental Panel on Climate Change [Masson-Delmotte, V., P. Zhai, A. Pirani, S.L. Connors, C. Péan, S. Berger, N. Caud, Y. Chen, L. Goldfarb, M.I. Gomis, M. Huang, K. Leitzell, E. Lonnoy, J.B.R. Matthews, T.K. Maycock, T. Waterfield, O. Yelekçi, R. Yu, and B. Zhou (eds.)]., Cambridge University Press, Cambridge, United Kingdom and New York, NY, USA, 923–1054, 2021.

Fuglestvedt, J., Berntsen, T., Myhre, G., Rypdal, K., and Skeie, R. B.: Climate forcing from the transport sectors, 875   Proceedings of the National Academy of Sciences, 105, 454–458, https://doi.org/10.1073/pnas.0702958104, 2008.

Fuglestvedt, J. S. and Berntsen, T. K.: A simple model for scenario studies of changes in global climate: Version 1.0, CICERO Center for International Climate and Environmental Research - Oslo, 1999.

Gasser, T., Crepin, L., Quilcaille, Y., Houghton, R. A., Ciais, P., and Obersteiner, M.: Historical CO_2 emissions from land use and land cover change and their uncertainty, Biogeosciences, 17, 4075–4101, https://doi.org/10.5194/bg-17-4075-2020, 880   2020.

Grewe, V.: A generalized tagging method, Geoscientific Model Development, 6, 247–253, https://doi.org/10.5194/gmd-6-247-2013, 2013.

Guivarch, C., Kriegler, E., Portugal-Pereira, J., Bosetti, V., Edmonds, J., Fischedick, M., Havlík, P., Jaramilo, P., Krey, V., Lecocq, F., Lucena, A. F. P., Meinshausen, M., Mirasgedis, S., O'Neill, B., Peters, G. P., Rogelj, J., Rose, S., Saheb, Y., 885   Strbac, G., Hammer Strømman, A., van Vuuren, D. P., and Zhou, N.: IPCC, 2022: Annex III: Scenarios and modelling methods, in: IPCC, 2022: Climate Change 2022: Mitigation of Climate Change. Contribution of Working Group III to the Sixth Assessment Report of the Intergovernmental Panel on Climate Change [P.R. Shukla, J. Skea, R. Slade, A. Al Khourdajie, R. van Diemen, D. McCollum, M. Pathak, S. Some, P. Vyas, R. Fradera, M. Belkacemi, A. Hasija, G. Lisboa, S. Luz, J. Malley, (eds.)], Cambridge University Press, Cambridge, United Kingdom and New York, NY, USA, 2022.

890   Harvey, D., Gregory, J., Hoffert, M., Atul, J., Lal, M., Leemans, R., Raper, S. C. B., Wigley, T. M. L., and de Wolde, J.: An introduction to Simple Climate Models used in the IPCC Second Assessment Report, 1997.

Hauglustaine, D., Paulot, F., Collins, W., Derwent, R., Sand, M., and Boucher, O.: Climate benefit of a future hydrogen economy, Commun Earth Environ, 3, 1–14, https://doi.org/10.1038/s43247-022-00626-z, 2022.

Höhne, N., Blum, H., Fuglestvedt, J., Skeie, R. B., Kurosawa, A., Hu, G., Lowe, J., Gohar, L., Matthews, B., Nioac de
895 Salles, A. C., and Ellermann, C.: Contributions of individual countries' emissions to climate change and their uncertainty, Climatic Change, 106, 359–391, https://doi.org/10.1007/s10584-010-9930-6, 2011.

Jenkins, S., Cain, M., Friedlingstein, P., Gillett, N., Walsh, T., and Allen, M. R.: Quantifying non-CO2 contributions to remaining carbon budgets, npj Clim Atmos Sci, 4, 1–10, https://doi.org/10.1038/s41612-021-00203-9, 2021.

Jia, H. and Quaas, J.: Nonlinearity of the cloud response postpones climate penalty of mitigating air pollution in polluted
900 regions, Nat. Clim. Chang., 13, 943–950, https://doi.org/10.1038/s41558-023-01775-5, 2023.

Joos, F. and Bruno, M.: Pulse response functions are cost-efficient tools to model the link between carbon emissions, atmospheric CO2 and global warming, Physics and Chemistry of the Earth, 21, 471–476, https://doi.org/10.1016/S0079-1946(97)81144-5, 1996.

Joos, F., Bruno, M., Fink, R., Siegenthaler, U., Stocker, T. F., Quéré, C. L., and Sarmiento, J. L.: An efficient and accurate
905 representation of complex oceanic and biospheric models of anthropogenic carbon uptake, 48, 397, https://doi.org/10.3402/tellusb.v48i3.15921, 1996.

Kikstra, J. S., Nicholls, Z. R. J., Smith, C. J., Lewis, J., Lamboll, R. D., Byers, E., Sandstad, M., Meinshausen, M., Gidden, M. J., Rogelj, J., Kriegler, E., Peters, G. P., Fuglestvedt, J. S., Skeie, R. B., Samset, B. H., Wienpahl, L., van Vuuren, D. P., van der Wijst, K.-I., Al Khourdajie, A., Forster, P. M., Reisinger, A., Schaeffer, R., and Riahi, K.: The IPCC Sixth
910 Assessment Report WGIII climate assessment of mitigation pathways: from emissions to global temperatures, Geoscientific Model Development, 15, 9075–9109, https://doi.org/10.5194/gmd-15-9075-2022, 2022.

Kretzschmar, J., Salzmann, M., Mülmenstädt, J., Boucher, O., and Quaas, J.: Comment on "Rethinking the Lower Bound on Aerosol Radiative Forcing," Journal of Climate, 30, 6579–6584, https://doi.org/10.1175/JCLI-D-16-0668.1, 2017.

Lamboll, R. D., Nicholls, Z. R. J., Smith, C. J., Kikstra, J. S., Byers, E., and Rogelj, J.: Assessing the size and uncertainty of
915 remaining carbon budgets, Nature Climate Change, 13, 1360–1367, https://doi.org/10.1038/s41558-023-01848-5, 2023.

Meinshausen, M., Raper, S. C. B., and Wigley, T. M. L.: Emulating coupled atmosphere-ocean and carbon cycle models with a simpler model, MAGICC6 – Part 1: Model description and calibration, Atmospheric Chemistry and Physics, 11, 1417–1456, https://doi.org/10.5194/acp-11-1417-2011, 2011.

Meinshausen, M., Vogel, E., Nauels, A., Lorbacher, K., Meinshausen, N., Etheridge, D. M., Fraser, P. J., Montzka, S. A.,
920 Rayner, P. J., Trudinger, C. M., Krummel, P. B., Beyerle, U., Canadell, J. G., Daniel, J. S., Enting, I. G., Law, R. M., Lunder, C. R., O'Doherty, S., Prinn, R. G., Reimann, S., Rubino, M., Velders, G. J. M., Vollmer, M. K., Wang, R. H. J., and Weiss, R.: Historical greenhouse gas concentrations for climate modelling (CMIP6), Geoscientific Model Development, 10, 2057–2116, https://doi.org/10.5194/gmd-10-2057-2017, 2017.

Meinshausen, M., Nicholls, Z. R. J., Lewis, J., Gidden, M. J., Vogel, E., Freund, M., Beyerle, U., Gessner, C., Nauels, A.,
925 Bauer, N., Canadell, J. G., Daniel, J. S., John, A., Krummel, P. B., Luderer, G., Meinshausen, N., Montzka, S. A., Rayner, P. J., Reimann, S., Smith, S. J., van den Berg, M., Velders, G. J. M., Vollmer, M. K., and Wang, R. H. J.: The shared socio-economic pathway (SSP) greenhouse gas concentrations and their extensions to 2500, Geoscientific Model Development, 13, 3571–3605, https://doi.org/10.5194/gmd-13-3571-2020, 2020.

Morice, C. P., Kennedy, J. J., Rayner, N. A., Winn, J. P., Hogan, E., Killick, R. E., Dunn, R. J. H., Osborn, T. J., Jones, P.
930 D., and Simpson, I. R.: An Updated Assessment of Near-Surface Temperature Change From 1850: The HadCRUT5 Data Set, Journal of Geophysical Research: Atmospheres, 126, e2019JD032361, https://doi.org/10.1029/2019JD032361, 2021.

Myhre, G., Fuglestvedt, J. S., Berntsen, T. K., and Lund, M. T.: Mitigation of short-lived heating components may lead to unwanted long-term consequences, Atmospheric Environment, 45, 6103–6106, https://doi.org/10.1016/j.atmosenv.2011.08.009, 2011.

935 Nicholls, Z. and Gieseke, R.: RCMIP Phase 1 Data (v2.0.0), https://doi.org/10.5281/zenodo.4016613, 2019.

Nicholls, Z., Meinshausen, M., Lewis, J., Corradi, M. R., Dorheim, K., Gasser, T., Gieseke, R., Hope, A. P., Leach, N. J., McBride, L. A., Quilcaille, Y., Rogelj, J., Salawitch, R. J., Samset, B. H., Sandstad, M., Shiklomanov, A., Skeie, R. B., Smith, C. J., Smith, S. J., Su, X., Tsutsui, J., Vega-Westhoff, B., and Woodard, D. L.: Reduced Complexity Model Intercomparison Project Phase 2: Synthesizing Earth System Knowledge for Probabilistic Climate Projections, Earth's
940 Future, 9, e2020EF001900, https://doi.org/10.1029/2020EF001900, 2021.

Nicholls, Z. R. J., Meinshausen, M., Lewis, J., Gieseke, R., Dommenget, D., Dorheim, K., Fan, C.-S., Fuglestvedt, J. S., Gasser, T., Golüke, U., Goodwin, P., Hartin, C., Hope, A. P., Kriegler, E., Leach, N. J., Marchegiani, D., McBride, L. A., Quilcaille, Y., Rogelj, J., Salawitch, R. J., Samset, B. H., Sandstad, M., Shiklomanov, A. N., Skeie, R. B., Smith, C. J., Smith, S., Tanaka, K., Tsutsui, J., and Xie, Z.: Reduced Complexity Model Intercomparison Project Phase 1: introduction
945 and evaluation of global-mean temperature response, Geoscientific Model Development, 13, 5175–5190, https://doi.org/10.5194/gmd-13-5175-2020, 2020.

Olivié, D. and Stuber, N.: Emulating AOGCM results using simple climate models, Clim Dyn, 35, 1257–1287, https://doi.org/10.1007/s00382-009-0725-2, 2010.

Osborn, T. J. and Wigley, T. M. L.: A simple model for estimating methane concentration and lifetime variations, Climate
950 Dynamics, 4/5, 181–193, 1994.

Paulot, F., Paynter, D., Naik, V., Malyshev, S., Menzel, R., and Horowitz, L. W.: Global modeling of hydrogen using GFDL-AM4.1: Sensitivity of soil removal and radiative forcing, International Journal of Hydrogen Energy, 46, 13446–13460, https://doi.org/10.1016/j.ijhydene.2021.01.088, 2021.

Peters, G. P., Aamaas, B., Berntsen, T., and Fuglestvedt, J. S.: The integrated global temperature change potential (iGTP)
955 and relationships between emission metrics, Environ. Res. Lett., 6, 044021, https://doi.org/10.1088/1748-9326/6/4/044021, 2011.

Raper, S. C. B., Gregory, J. M., and Osborn, T. J.: Use of an upwelling-diffusion energy balance climate model to simulate and diagnose A/OGCM results, Climate Dynamics, 17, 601–613, https://doi.org/10.1007/PL00007931, 2001.

Sand, M., Skeie, R. B., Sandstad, M., Krishnan, S., Myhre, G., Bryant, H., Derwent, R., Hauglustaine, D., Paulot, F., Prather,
960 M., and Stevenson, D.: A multi-model assessment of the Global Warming Potential of hydrogen, Commun Earth Environ, 4, 1–12, https://doi.org/10.1038/s43247-023-00857-8, 2023.

Sanderson, B.: The role of prior assumptions in carbon budget calculations, Earth System Dynamics, 11, 563–577, https://doi.org/10.5194/esd-11-563-2020, 2020.

Saunois, M., Stavert, A. R., Poulter, B., Bousquet, P., Canadell, J. G., Jackson, R. B., Raymond, P. A., Dlugokencky, E. J.,
965 Houweling, S., Patra, P. K., Ciais, P., Arora, V. K., Bastviken, D., Bergamaschi, P., Blake, D. R., Brailsford, G., Bruhwiler, L., Carlson, K. M., Carrol, M., Castaldi, S., Chandra, N., Crevoisier, C., Crill, P. M., Covey, K., Curry, C. L., Etiope, G., Frankenberg, C., Gedney, N., Hegglin, M. I., Höglund-Isaksson, L., Hugelius, G., Ishizawa, M., Ito, A., Janssens-Maenhout, G., Jensen, K. M., Joos, F., Kleinen, T., Krummel, P. B., Langenfelds, R. L., Laruelle, G. G., Liu, L., Machida, T., Maksyutov, S., McDonald, K. C., McNorton, J., Miller, P. A., Melton, J. R., Morino, I., Müller, J., Murguia-Flores, F., Naik,
970 V., Niwa, Y., Noce, S., O'Doherty, S., Parker, R. J., Peng, C., Peng, S., Peters, G. P., Prigent, C., Prinn, R., Ramonet, M.,

Regnier, P., Riley, W. J., Rosentreter, J. A., Segers, A., Simpson, I. J., Shi, H., Smith, S. J., Steele, L. P., Thornton, B. F., Tian, H., Tohjima, Y., Tubiello, F. N., Tsuruta, A., Viovy, N., Voulgarakis, A., Weber, T. S., van Weele, M., van der Werf, G. R., Weiss, R. F., Worthy, D., Wunch, D., Yin, Y., Yoshida, Y., Zhang, W., Zhang, Z., Zhao, Y., Zheng, B., Zhu, Q., Zhu, Q., and Zhuang, Q.: The Global Methane Budget 2000–2017, Earth System Science Data, 12, 1561–1623, https://doi.org/10.5194/essd-12-1561-2020, 2020.

Schlesinger, M. E. and Jiang, X.: Simple Model Representation of Atmosphere-Ocean GCMs and Estimation of the Time Scale of C02-Induced Climate Change, Journal of Climate, 3, 1297–1315, https://doi.org/10.1175/1520-0442(1990)003<1297:SMROAO>2.0.CO;2, 1990.

Schlesinger, M. E., Jiang, X., and Charlson, R. J.: Implication of Anthropogenic Atmospheric Sulphate for the Sensitivity of the Climate System, 1992.

Schneider, S. H. and Thompson, S. L.: Atmospheric CO2 and climate: Importance of the transient response, Journal of Geophysical Research: Oceans, 86, 3135–3147, https://doi.org/10.1029/JC086iC04p03135, 1981.

von Schuckmann, K., Minière, A., Gues, F., Cuesta-Valero, F. J., Kirchengast, G., Adusumilli, S., Straneo, F., Ablain, M., Allan, R. P., Barker, P. M., Beltrami, H., Blazquez, A., Boyer, T., Cheng, L., Church, J., Desbruyeres, D., Dolman, H., Domingues, C. M., García-García, A., Giglio, D., Gilson, J. E., Gorfer, M., Haimberger, L., Hakuba, M. Z., Hendricks, S., Hosoda, S., Johnson, G. C., Killick, R., King, B., Kolodziejczyk, N., Korosov, A., Krinner, G., Kuusela, M., Landerer, F. W., Langer, M., Lavergne, T., Lawrence, I., Li, Y., Lyman, J., Marti, F., Marzeion, B., Mayer, M., MacDougall, A. H., McDougall, T., Monselesan, D. P., Nitzbon, J., Otosaka, I., Peng, J., Purkey, S., Roemmich, D., Sato, K., Sato, K., Savita, A., Schweiger, A., Shepherd, A., Seneviratne, S. I., Simons, L., Slater, D. A., Slater, T., Steiner, A. K., Suga, T., Szekely, T., Thiery, W., Timmermans, M.-L., Vanderkelen, I., Wjiffels, S. E., Wu, T., and Zemp, M.: Heat stored in the Earth system 1960–2020: where does the energy go?, Earth System Science Data, 15, 1675–1709, https://doi.org/10.5194/essd-15-1675-2023, 2023.

Sherwood, S. C., Webb, M. J., Annan, J. D., Armour, K. C., Forster, P. M., Hargreaves, J. C., Hegerl, G., Klein, S. A., Marvel, K. D., Rohling, E. J., Watanabe, M., Andrews, T., Braconnot, P., Bretherton, C. S., Foster, G. L., Hausfather, Z., von der Heydt, A. S., Knutti, R., Mauritsen, T., Norris, J. R., Proistosescu, C., Rugenstein, M., Schmidt, G. A., Tokarska, K. B., and Zelinka, M. D.: An Assessment of Earth's Climate Sensitivity Using Multiple Lines of Evidence, Reviews of Geophysics, 58, e2019RG000678, https://doi.org/10.1029/2019RG000678, 2020.

Siegenthaler, U. and Joos, F.: Use of a simple model for studying oceanic tracer distributions and the global carbon cycle, Tellus B, 44, 186–207, https://doi.org/10.1034/j.1600-0889.1992.t01-2-00003.x, 1992.

Skeie, R. B., Fuglestvedt, J., Berntsen, T., Lund, M. T., Myhre, G., and Rypdal, K.: Global temperature change from the transport sectors: Historical development and future scenarios, Atmospheric Environment, 43, 6260–6270, https://doi.org/10.1016/j.atmosenv.2009.05.025, 2009.

Skeie, R. B., Berntsen, T., Aldrin, M., Holden, M., and Myhre, G.: A lower and more constrained estimate of climate sensitivity using updated observations and detailed radiative forcing time series, Earth System Dynamics, 5, 139–175, https://doi.org/10.5194/esd-5-139-2014, 2014.

Skeie, R. B., Fuglestvedt, J., Berntsen, T., Peters, G. P., Andrew, R., Allen, M., and Kallbekken, S.: Perspective has a strong effect on the calculation of historical contributions to global warming, Environ. Res. Lett., 12, 024022, https://doi.org/10.1088/1748-9326/aa5b0a, 2017.

Skeie, R. B., Berntsen, T., Aldrin, M., Holden, M., and Myhre, G.: Climate sensitivity estimates – sensitivity to radiative forcing time series and observational data, Earth System Dynamics, 9, 879–894, https://doi.org/10.5194/esd-9-879-2018, 2018.

Skeie, R. B., Myhre, G., Hodnebrog, Ø., Cameron-Smith, P. J., Deushi, M., Hegglin, M. I., Horowitz, L. W., Kramer, R. J., Michou, M., Mills, M. J., Olivié, D. J. L., Connor, F. M. O., Paynter, D., Samset, B. H., Sellar, A., Shindell, D., Takemura, T., Tilmes, S., and Wu, T.: Historical total ozone radiative forcing derived from CMIP6 simulations, npj Clim Atmos Sci, 3, 1–10, https://doi.org/10.1038/s41612-020-00131-0, 2020.

Skeie, R. B., Peters, G. P., Fuglestvedt, J., and Andrew, R.: A future perspective of historical contributions to climate change, Climatic Change, 164, 24, https://doi.org/10.1007/s10584-021-02982-9, 2021.

Skeie, R. B., Hodnebrog, Ø., and Myhre, G.: Trends in atmospheric methane concentrations since 1990 were driven and modified by anthropogenic emissions, Commun Earth Environ, 4, 1–14, https://doi.org/10.1038/s43247-023-00969-1, 2023.

Smith, C., Forster, P., Palmer, M., Collins, B., Leach, N., Watanabe, M., Berger, S., Hall, B., Zelinka, M., Lunt, D., Cain, M., Harris, G., and Ringer, M.: IPCC WGI AR6 Chapter 7, , https://doi.org/10.5281/zenodo.5211358, 2021a.

Smith, C. J., Kramer, R. J., Myhre, G., Alterskjær, K., Collins, W., Sima, A., Boucher, O., Dufresne, J.-L., Nabat, P., Michou, M., Yukimoto, S., Cole, J., Paynter, D., Shiogama, H., O'Connor, F. M., Robertson, E., Wiltshire, A., Andrews, T., Hannay, C., Miller, R., Nazarenko, L., Kirkevåg, A., Olivié, D., Fiedler, S., Lewinschal, A., Mackallah, C., Dix, M., Pincus, R., and Forster, P. M.: Effective radiative forcing and adjustments in CMIP6 models, Atmospheric Chemistry and Physics, 20, 9591–9618, https://doi.org/10.5194/acp-20-9591-2020, 2020.

Smith, C. J., Nicholls, Z. R. J., Armour, K., Forster, P. M. de F., Meinshausen, M., Palmer, M. D., and Watanabe, M.: The Earth's Energy Budget, Climate Feedbacks, and Climate Sensitivity Supplementary Material. In [Masson-Delmotte, V., P. Zhai, A. Pirani, S.L. Connors, C. Péan, S. Berger, N. Caud, Y. Chen, L. Goldfarb, M.I. Gomis, M. Huang, K. Leitzell, E. Lonnoy, J.B.R. Matthews, T.K. Maycock, T. Waterfield, O. Yelekçi, R. Yu, and B. Zhou (eds.)]. Available from https://www.ipcc.ch/., in: Climate Change 2021: The Physical Science Basis. Contribution of Working Group I to the Sixth Assessment Report of the Intergovernmental Panel on Climate Change [Masson-Delmotte, V., P. Zhai, A. Pirani, S.L. Connors, C. Péan, S. Berger, N. Caud, Y. Chen, L. Goldfarb, M.I. Gomis, M. Huang, K. Leitzell, E. Lonnoy, J.B.R. Matthews, T.K. Maycock, T. Waterfield, O. Yelekçi, R. Yu, and B. Zhou (eds.)]. Available from https://www.ipcc.ch/., 2021b.

Stevenson, D. S., Zhao, A., Naik, V., O'Connor, F. M., Tilmes, S., Zeng, G., Murray, L. T., Collins, W. J., Griffiths, P. T., Shim, S., Horowitz, L. W., Sentman, L. T., and Emmons, L.: Trends in global tropospheric hydroxyl radical and methane lifetime since 1850 from AerChemMIP, Atmospheric Chemistry and Physics, 20, 12905–12920, https://doi.org/10.5194/acp-20-12905-2020, 2020.

Tian, H., Xu, R., Canadell, J. G., Thompson, R. L., Winiwarter, W., Suntharalingam, P., Davidson, E. A., Ciais, P., Jackson, R. B., Janssens-Maenhout, G., Prather, M. J., Regnier, P., Pan, N., Pan, S., Peters, G. P., Shi, H., Tubiello, F. N., Zaehle, S., Zhou, F., Arneth, A., Battaglia, G., Berthet, S., Bopp, L., Bouwman, A. F., Buitenhuis, E. T., Chang, J., Chipperfield, M. P., Dangal, S. R. S., Dlugokencky, E., Elkins, J. W., Eyre, B. D., Fu, B., Hall, B., Ito, A., Joos, F., Krummel, P. B., Landolfi, A., Laruelle, G. G., Lauerwald, R., Li, W., Lienert, S., Maavara, T., MacLeod, M., Millet, D. B., Olin, S., Patra, P. K., Prinn, R. G., Raymond, P. A., Ruiz, D. J., van der Werf, G. R., Vuichard, N., Wang, J., Weiss, R. F., Wells, K. C., Wilson, C., Yang, J., and Yao, Y.: A comprehensive quantification of global nitrous oxide sources and sinks, Nature, 586, 248–256, https://doi.org/10.1038/s41586-020-2780-0, 2020.

Torvanger, A., Grimstad, A.-A., Lindeberg, E., Rive, N., Rypdal, K., Skeie, R. B., Fuglestvedt, J., and Tollefsen, P.: Quality of geological CO2 storage to avoid jeopardizing climate targets, Climatic Change, 114, 245–260, https://doi.org/10.1007/s10584-012-0447-z, 2012.

Torvanger, A., Lund, M. T., and Rive, N.: Carbon capture and storage deployment rates: needs and feasibility, Mitig Adapt Strateg Glob Change, 18, 187–205, https://doi.org/10.1007/s11027-012-9357-7, 2013.

Tronstad Lund, M., Eyring, V., Fuglestvedt, J., Hendricks, J., Lauer, A., Lee, D., and Righi, M.: Global-Mean Temperature Change from Shipping toward 2050: Improved Representation of the Indirect Aerosol Effect in Simple Climate Models, Environ. Sci. Technol., 46, 8868–8877, https://doi.org/10.1021/es301166e, 2012.

Warwick, N. J., Archibald, A. T., Griffiths, P. T., Keeble, J., O'Connor, F. M., Pyle, J. A., and Shine, K. P.: Atmospheric composition and climate impacts of a future hydrogen economy, Atmospheric Chemistry and Physics, 23, 13451–13467, https://doi.org/10.5194/acp-23-13451-2023, 2023.

Wigley, T. M. L. and Raper, S. C. B.: Implications for climate and sea level of revised IPCC emissions scenarios, Nature, 357, 293–300, https://doi.org/10.1038/357293a0, 1992.

Winterstein, F., Tanalski, F., Jöckel, P., Dameris, M., and Ponater, M.: Implication of strongly increased atmospheric methane concentrations for chemistry–climate connections, Atmospheric Chemistry and Physics, 19, 7151–7163, https://doi.org/10.5194/acp-19-7151-2019, 2019.